Validation of the HITRAN 2016 and GEISA 2015 line lists using ACE-FTS solar occultation observations

Kevin Olsen, C. D. Boone, G. C. Toon, Franck Montmessin, A. A. Fedorova, O. Korablev, Alexander Trokhimovskiy

Highlights

- Updated versions of GEISA 2015 and HITRAN 2016 line lists are validated using terrestrial solar occultation spectra from ACE-FTS.
- Spectroscopic parameters for CO_2 and H_2O are improved in both line lists.
- The primary difference we observe between the two line lists comes from O_3 absorption features near 3850 cm^{-1} and from several CH4 absorption lines in the regions 2800-3200 cm^{-1} and 4000-4300 cm^{-1}.

Validation of the HITRAN 2016 and GEISA 2015 line lists using ACE-FTS solar occultation observations

K. S. Olsen[a,*], C. D. Boone[b], G. C. Toon[c], F. Montmessin[a], A. A. Fedorova[d], O. Korablev[d], A. Trokhimovskiy[d]

[a] *Laboratoire Atmosphères, Milieux, Observations Spatiales (LATMOS), Université Versailles St Quentin en Yvelines, Guyancourt 78280, France.*
[b] *Department of Chemistry, University of Waterloo, Waterloo ON N2L 3G1, Canada.*
[c] *Jet Propulsion Laboratory (JPL), California Institute of Technology, Pasadena CA 91109, USA.*
[d] *Space Research Institute (IKI), Russian Academy of Sciences, Moscow 117997, Russia.*

Abstract

The ExoMars Trace Gas Orbiter (TGO) began its nominal science phase at Mars in April 2018, following releases of editions to two major spectroscopic line lists: GEISA 2015 (Gestion et Etude des Informations Spectroscopiques Atmosphériques: Management and Study of Atmospheric Spectroscopic Information), and HITRAN 2016 (High Resolution Transmission). This work evaluates both line lists over the spectral region between 2325–4350 cm^{-1} using terrestrial solar occultation observations made by the Atmospheric Chemistry Experiment Fourier Transform Spectrometer (ACE-FTS). This spectral region is targeted on Mars by two complementary solar occultation instruments on TGO that will monitor temperature and pressure, aerosols,

*Corresponding author
Email addresses: kevin.olsen@latmos.ipsl.fr (K. S. Olsen), cboone@scisat.ca (C. D. Boone), geoffrey.c.toon@jpl.nasa.gov (G. C. Toon), franck.montmessin@latmos.ipsl.fr (F. Montmessin), fedorova@iki.rssi.ru (A. A. Fedorova), korab@iki.rssi.ru (O. Korablev), trokh@iki.rssi.ru (A. Trokhimovskiy)

Preprint submitted to Journal of Quantitative Spectroscopy and Radiative Transfer July 30, 2019

the abundance of CO_2, CO, H_2O, HDO, CH_4, and other undetected trace gases. Major updates to GEISA 2015 and HITRAN 2016, with respect to previous editions, have been focused on CO_2 absorption features in support of Earth-observing missions to monitor greenhouse. Since CO_2 is the dominant absorber on Mars, making up 96.5% of the atmosphere, validating the updated line lists is critically important before their deployment for ExoMars. We report that updated CO_2 parameters make significant improvements to spectral fits made when using both line lists. Several updates to H_2O lines in both line lists also show improvement. The primary difference we observe between the two line lists comes from O_3 absorption features near 3850 cm^{-1} and from several CH_4 absorption lines in the regions 2800–3200 cm^{-1} and 4000–4300 cm^{-1}. Because of these differences, we find that using HITRAN 2016 tends to result in better spectral fits, especially below 30 km, than using GEISA 2015 in this spectral region. Differences are strongly reduced with increasing altitude ($>$ 40 km) as pressure and gas abundance falls off. It was also discovered that several new errors in both new editions of GEISA and HITRAN were introduced since the HITRAN 2012.
Keywords: ACE-FTS, HITRAN, GEISA, ExoMars, line-list

1. Introduction

New editions of two major spectroscopic line lists have been recently released: Gestion et Etude des Informations Spectroscopiques Atmosphériques: Management and Study of Atmospheric Spectroscopic Information (GEISA) in 2015 (Jacquinet-Husson et al., 2016); and High Resolution Transmission (HITRAN) in 2016 (Gordon et al., 2017). Here, we present a comparison

of spectral fits to solar occultation measurements of the Earth's atmosphere made by the Canadian Space Agency's (CSA's) Atmospheric Chemistry Experiment (ACE) Fourier transform spectrometer (FTS) using both line lists. This work was motivated by the arrival of the European Space Agency (ESA) and Roscosmos' ExoMars Trace Gas Orbiter (TGO) at Mars in October 2016. The TGO carries two infrared remote sensing instrument suites, the Atmospheric Chemistry Suite (ACS) (Korablev et al., 2018) and the Nadir and Occultation for Mars Discovery (NOMAD) (Vandaele et al., 2018). Both instrument suites carry channels dedicated to making solar occultation observations at Mars in the infrared wavenumber range of 2325–4350 cm^{-1}.

The controversial observation of methane (CH_4) in the Martian atmosphere (Formisano et al., 2004; Krasnopolsky et al., 2004; Mumma et al., 2009; Webster et al., 2015, 2018; Giuranna et al., 2019) is one of the key motivations of the ExoMars mission (Zurek et al., 2011; Vandaele et al., 2015; Korablev et al., 2018). NOMAD and ACS will search for CH_4 by making solar occultation observations of its ν_2 vibration-rotation band centred near 3000 cm^{-1}, which hosts the strongest absorption features available to both instruments. A key benefit of searching for CH_4 in this region is that it is relatively clear of interfering absorption lines from CO_2. There is a recently-observed, weak vibration-rotation band of carbon dioxide (CO_2) that overlaps CH_4 in this region (Bertaux et al., 2008; Villanueva et al., 2008) and one of our specific objectives was to evaluate its spectroscopic parameters in GEISA 2015 and HITRAN 2016.

ACS and NOMAD will also make detailed measurements of water vapour (H_2O), having the capability of distinguishing isotopologues. The ratio of

HDO to H_2O has been used as a critical indicator of the Martian climate in the ancient past (e.g., Encrenaz et al., 2018; Krasnopolsky, 2015). The relative abundance of HDO on Mars is enriched relative to Earth, which supports mechanisms for hydrogen escape from the atmosphere, which are preferential towards the lighter isotope (Clarke et al., 2017). ACS and NOMAD will be able measure the vertical structure of H_2O isotopologues, and monitor their ratios seasonally, spatially, and vertically.

In support of the study of Earth's contemporary climate, and the carbon cycle, with the Orbiting Carbon Observatory (OCO-2) (Crisp et al., 2004, 2017), the Greenhouse gases Observing SATellite (GOSAT) (Yokota et al., 2009), and the Total Carbon Column Observing Network (TCCON) (Wunch et al., 2011), a large effort has been undertaken to refine and reduce the uncertainty of the spectroscopic parameters of CO_2. While the surface pressure of Mars is only between 550–720 Pa, roughly 0.5–0.7% of Earth's, the volume mixing ratio of CO_2 is 0.965, or 2400 times that on Earth (400 ppmv). Therefore, CO_2 absorption lines in Mars solar occultation spectra will be deeper and broader than for spectra recorded at Earth, and small changes in the spectroscopic parameters may have a large impact on trace gas retrievals made at Mars.

Our goal was to evaluate the new CO_2, H_2O, and CH_4 parameters by looking at whether their impact when fitting terrestrial spectra was positive or negative. We have performed spectral fitting for 125 sets of ACE-FTS occultation spectra (resolution of 0.02 cm^{-1}) over 50 spectral windows covering the spectral range of 2430–4450 cm^{-1} using the HITRAN 2012, HITRAN 2016, and GEISA 2015 line lists.

HITRAN 2016 and GEISA 2015 are compilations of data sources, many of which are shared. One of our most important results is that the updated CO_2 parameters for some of the stronger vibration-rotation bands, especially those centred at 3550 cm^{-1} result in strongly improved spectral fits when using either HITRAN 2016 or GEISA 2015. However, we have also found that there are large differences in the spectroscopic parameters of ozone (O_3), CH_4, and H_2O between the two data sets, and that using HITRAN 2016 leads to improved spectral fits compared to GEISA 2015. This result is significant since methane is one of the strongest absorbers in the Earth's atmosphere, and is one of the most variable gases. Methane is of key importance for TGO, as ACS and NOMAD both aspire to make its irregular and controversial detection in the Martian atmosphere definitive. However, at this time no methane features have been observed at Mars by TGO instruments (Korablev et al., 2019).

While individual contributions to the line lists are validated, they are often done in laboratory settings, observing controlled gas samples, rather than with observations of an atmosphere (e.g., Jacquinet-Husson et al., 2016; Gordon et al., 2017, and references therein). Bailey (2009) previously made a direct comparison between H_2O transitions in older versions of GEISA and HITRAN, and qualitatively showed their differences using modelled spectra for Venus at high temperatures and above 4000 cm^{-1}. A comprehensive validation of the GEISA line list was done using TCCON and the Infrared Atmospheric Sounding Interferometer (IASI) (Clerbaux et al., 2009) by Armante et al. (2016). They describe a technique used to determine whether spectroscopic parameters should be used to update the GEISA database based

on comparisons of computed spectra to observations. They specifically show H_2O and HDO in the ExoMars region of interest and highlight improvements since GEISA 2011. They also compare CH_4 lines above 6000 cm^{-1} to HITRAN 2012 and note an improvement to the residuals. This method was used in the compilation of GEISA 2015 (Jacquinet-Husson et al., 2016).

A comprehensive validation of the HITRAN 2012 line list was undertaken by Toon et al. (2016) using the MkIV balloon-borne FTS (Toon, 1991). They divided the spectral region between 670–5620 cm^{-1} into fitting windows and quantitatively evaluated the best-fit residuals across the spectral range and with altitude for several versions of HITRAN released since 2000. They noted specific errors in the data base, where improvements were made, and where previous versions performed better. Their work was influential on the compilation of the latest version of HITRAN evaluated here (Gordon et al., 2017). Updates to Toon et al. (2016) are included in Toon (2019) and include evaluation of HITRAN 2016 and the TCCON internal line list, validation with laboratory spectra, and a specific analysis of CO_2 features. This work follows Toon et al. (2016) by using a similar quantitative evaluation technique and covering part of the same spectral region.

2. HITRAN 2016

The HITRAN (high-resolution transmission molecular absorption) database was first compiled for the Air Force Geophysics Laboratory (AFGL) by McClatchey et al. (1973) and major updated editions have been released on a four year cycle since 1992 (Rothman et al., 1992). The 2016 version of the HITRAN database (Gordon et al., 2017) describes changes made since the 2012

edition (Rothman et al., 2013). Among the most significant additions to the database have been the inclusion of spectroscopic parameters for collision-induced broadening from non-nitrogen based atmospheres and for non-Voigt line profiles (Wilzewski et al., 2016). The need for line broadening parameters in atmospheres primarily composed of gases other than N_2 has been motivated by extra-terrestrial spectroscopic applications, *e.g.,* Mars, which is 96% CO_2. HITRAN 2016 includes a sparse set of broadening parameters for atmospheres composed of H_2, He, or CO_2 for a subset of gases that includes CO, OCS, SO_2, NH_3, HF and HCl, which are all sought at Mars by the ExoMars TGO. For very high-resolution applications, HITRAN 2016 also includes parameters for the speed-dependent Voigt, Galatry, and Hartman-Tran line shapes. These are again only available for a subset of wavenumbers and only for H_2O, CO, H_2, O_2, N_2O, HF and HCl. Because of the complexity of the newly included parameters, newly-developed online tools are now used to create user-defined database versions. The 2016 version also expands the list of available molecules with the addition of C_2N_2 and $COCl_2$. While the number of additional lines, and the number of lines for which more accurate measurements have been made, is vast, we will primarily focus on key species relevant to Earth and Mars: CO_2, H_2O and CH_4.

For CO_2, Gordon et al. (2017) identifies the imperative for high-accuracy spectroscopic parameters driven by GOSAT, OCO-2, TCCON, and others, and identifies validated improvements between the 2008 and 2012 versions of the HITRAN database (Toon et al., 2016). The 2012 version of the database was largely built on theoretical fits of the effective Hamiltonian or effective dipole moments, compiled as the CDSD-296 database (Tashkun et al., 2015),

supplemented by higher-accuracy experimental measurements made by Toth et al. (2007, 2008a,b). The line intensity calculations in CDSD-296 have high uncertainties (∼20%) and two new sets of theoretical computation have been produced: the Ames list (Huang et al., 2014) and the UCL-IAO list (Zak et al., 2016). These have been extensively validated experimentally, and Gordon et al. (2017) refers to 14 such studies that show that the UCL-IAO list tends to be more accurate, and that the uncertainties for the 2016 version of HITRAN can be pushed down to the order of 0.5%. However, the majority of the experimental work focuses on important CO_2 bands for Earth observation (*e.g.*, for OCO-2) that lie outside the range of high-resolution solar occultation experiments on TGO, above 5000 cm^{-1} (near 1.6 and 2 µm). Only laboratory measurements presented in Lyulin et al. (2012) and Durry et al. (2010) cover the 2300–4400 cm^{-1} range, and the latter only does so near 3730 cm^{-1}. The 2016 HITRAN line list for CO_2 between 2300–4400 cm^{-1} is a combination of CDSD-296 theoretical calculations(Tashkun et al., 2015), UCL-IAO or Ames theoretical calculations where better or newly available (Huang et al., 2014; Zak et al., 2016), and laboratory measurements where available and with low enough uncertainty (e.g., Toth et al., 2008b; Durry et al., 2010; Lyulin et al., 2012).

For H_2O, the HITRAN 2012 line list was made up of *ab initio* calculations that comprised the BT2 line list (Barber et al., 2006), with updates, where available, from calculations using a more accurate method (Lodi et al., 2011; Lodi and Tennyson, 2012). Newer calculations using the methodology of Lodi and Tennyson (2012) have been made as part of an effort by the International Union of Pure and Applied Chemistry (IUPAC) task group (Tennyson et al.,

2009, and references therein). The new calculations have been validated experimentally by Birk et al. (2017) and the results have been used to update both the IUPAC database and the HITRAN line list. Extensive laboratory measurements have also been made for the German Aerospace Agency (DLR) in the spectral range between 1850–4000 cm^{-1} by Loos et al. (2017a,b). When available, these replace the calculated line strengths of IUPAC and Lodi and Tennyson (2012).

The CH_4 data in HITRAN 2012 was comprised of the data set described in Brown et al. (2013), which was a combination of theoretical calculations and experimental measurements. This data set replaced over 70% of the HITRAN 2008 line list for CH_4 (Rothman et al., 2009). However, analysis of high-resolution solar occultation measurements in the Earth's atmosphere made by the MkIV interferometer (Toon, 1991) determined that there were still several errors and omissions in the HITRAN 2012 CH_4 data (Toon et al., 2016), especially in the spectral region of the ν_2 transition critical to ExoMars, near 3000 cm^{-1}. Errors that were identified were replaced by either the HITRAN 2008 values, or computations made by Tyuterev et al. (2013). Several laboratory studies have been recently undertaken, but the results have not yet been incorporated into the HITRAN line list, but an update to the 2016 edition is expected in the interim (Gordon et al., 2017).

3. GEISA 2015

The GEISA line list was first compiled in the early 1970s at the Laboratoire de Météorologie Dynamique (LMD) to support their radiative transfer investigations (Chédin et al., 1982). Key motivations for the compilation

were to include new gases important for planetary atmospheric applications, and to co-develop software tools to easily use the database. One distinguishing feature is to treat certain isotopologues with distinct symmetries as independent species (such as HDO for H_2O and CH_3D for CH_4) (Jacquinet-Husson et al., 2016). Comparing the available gases in current versions of GEISA and HITRAN, GeH_4, C_3H_8, C_3H_4, and C_6H_6 are unique to GEISA, while HOBr, O, H_2, and CS are unique to HITRAN. There are also several minor isotopologues of trace gases unique to both. Updates to GEISA are made after evaluating the relevance of new data, the efficiency of including it, and after undergoing a validation process as described in Armante et al. (2016).

For CO_2, the GEISA 2011 database was replaced by the CDSD-296 database (Tashkun et al., 2015). CDSD-296 is also the primary source of CO_2 parameters in the 2016 edition of HITRAN. GEISA also contains three isotopologues not contained in CDSD-296 from laboratory measurements by Jacquemart et al. (2012); Lyulin et al. (2012) (and others at at higher wavenumbers than 4400 cm^{-1}).

Extensive updates to H_2O were made empirically for GEISA 2015 by a consortium of eight laboratories, nearly tripling the number of available lines since the 2011 edition. In the spectral region of interest to ExoMars ($\sim$2300–4400 cm$-$1), these measurements were made by the Laboratoire Inter-Universitaire des Systèmes Atmosphériques (LISA), the Institute of Atmospheric Optics (IAO), and University College, London (Jacquinet-Husson et al., 2016). Updates to $H_2^{16}O$ come from (Coudert et al., 2014), and updates for $H_2^{17}O$ and $H_2^{18}O$ come from Lodi et al. (2011); Lodi and Tennyson (2012)

and the IUPAC efforts, which is the same source as for HITRAN 2016. These were supplemented or updated by measurements made by Coudert and Chelin (2016). GEISA 2015 also newly includes lines for two isotopologues of D_2O not included in HITRAN.

Updates to CH_4 in this spectral range mainly come from the work of Niederer et al. (2013); Nikitin et al. (2013) which use the same methodology as Brown et al. (2013) (HITRAN 2012). The validation work of Armante et al. (2016) showed some imprecision in the new parameters, resulting in some CH_4 lines from GEISA 2011 being retained.

4. Methodology

In this study, we break the wavenumber range of the ExoMars solar occultation spectrometers up into discrete fitting windows and analyze terrestrial solar occultation spectra recorded by ACE-FTS using the Jet Propulsion Laboratory Gas Fitting (GFIT or GGG) software suite. 125 occultations were analyzed. During an occultation, a series of observations of the sun are made while the limb of the atmosphere lies between the solar disk and the instrument. For each window, residuals were computed for each altitude level. The means of the residuals were taken at levels of equal pressure, and the root-mean-square (RMS) and standard deviation (σ) were computed for each fitting window. The means of the residuals were taken, rather than computing the residuals of mean spectra, due to variations in line depths between occultations, especially for CH_4 lines. In general, the lower the results RMS of the mean residuals is, the more accurate the spectroscopic parameters used in the fitting are. This methodology is very similar to that used by

Toon et al. (2016) who analyzed MkIV spectra.

ACE-FTS is a compact, double-pass interferometer with a spectral resolution of 0.02 cm^{-1} and a spectral range of 750–4400 cm^{-1}. It has been operating continuously in low-Earth orbit since 2003. The 125 ACE-FTS occultations analyzed were recorded between 2004 and 2012 and are unrestricted in longitude and season. Most observations are at high latitudes due to the ACE orbit (650 km with an inclination of 74°). A sequence of measurements is made with an observation every 1–6.5 km, and on average every 4 km. Two detectors provide an simultaneous spectral range of 750–4400 cm^{-1} (Bernath et al., 2005).

Spectral fitting in this study was done with GGG, which is also being used to analyze solar occultation observations made by ACS on ExoMars. GGG is developed from early Occultation Display Spectra (ODS) used by the ATMOS FTS that flew on the space shuttle (Norton and Rinsland, 1991; Irion et al., 2002). It is a robust software suite adaptable for solar occultations (Toon, 1991; Toon et al., 2016; Olsen et al., 2015), ground based observations (Wunch et al., 2011), or laboratory measurements. For each altitude and each fitting window, GGG computes a spectrum from a set of parameters that include the calculated optical path, vertical profiles of pressure and temperature, and *a priori* gas volume mixing ratio (VMR) vertical profiles. GGG then performs non-linear least squares fitting to adjust VMR scaling factors (as well as other optional parameters such as continuum level and frequency shift) to obtain a best fit. Retrieved VMR vertical profiles can be obtained by inverting the matrix of VMR scale factors for each target gas at each altitude, with the matrix of slant paths (Sen et al., 1996; Wunch et al.,

2011).

A priori temperature, pressure, and specific humidity vertical profiles were derived from National Centers for Environmental Prediction (NCEP) reanalysis data (Kalnay et al., 1996) up to 40 km. The US standard atmosphere was used above 40 km.

For this work, we consider the fitting residuals for each window and focus on three pressure levels where we take the means of the residuals: 0.052, 0.0029, and 0.00023 atm, corresponding to 20,40 and 60 km respectively. For each occultation, fitting was performed at all altitudes and in all spectral windows. The closest altitude level to the predetermined pressure levels was identified. The residuals were computed for each window and the RMS and standard deviation were computed from the residual as:

$$\begin{aligned} \mathrm{RMS}^2 &= \sum x_i^2/N, \\ \sigma^2 &= \sum (x_i - \bar{x})^2/(N-1), \end{aligned} \tag{1}$$

where N is the number of spectral points, x_i is the residual value at the i^{th} spectral point, and $\bar{x}$ is the mean of the residual. In general, for this application $\bar{x} \sim 0$ and $\mathrm{RMS}^2 \sim \sigma^2$. For strong deviations between the computed and observed spectra, σ^2 will reflect the magnitude of deviations from the mean of the residuals, while the RMS will reflect the deviation from zero, which is the expected outcome for a good fit. Therefore, the presented results will use the RMS values.

The fitting windows used are given in Tables 1 and 2, and panel a in Figure 1 shows their distribution over a sample of ACE-FTS solar occultation transmission spectrum. Panels b–e in Figure 1 illustrate the locations and

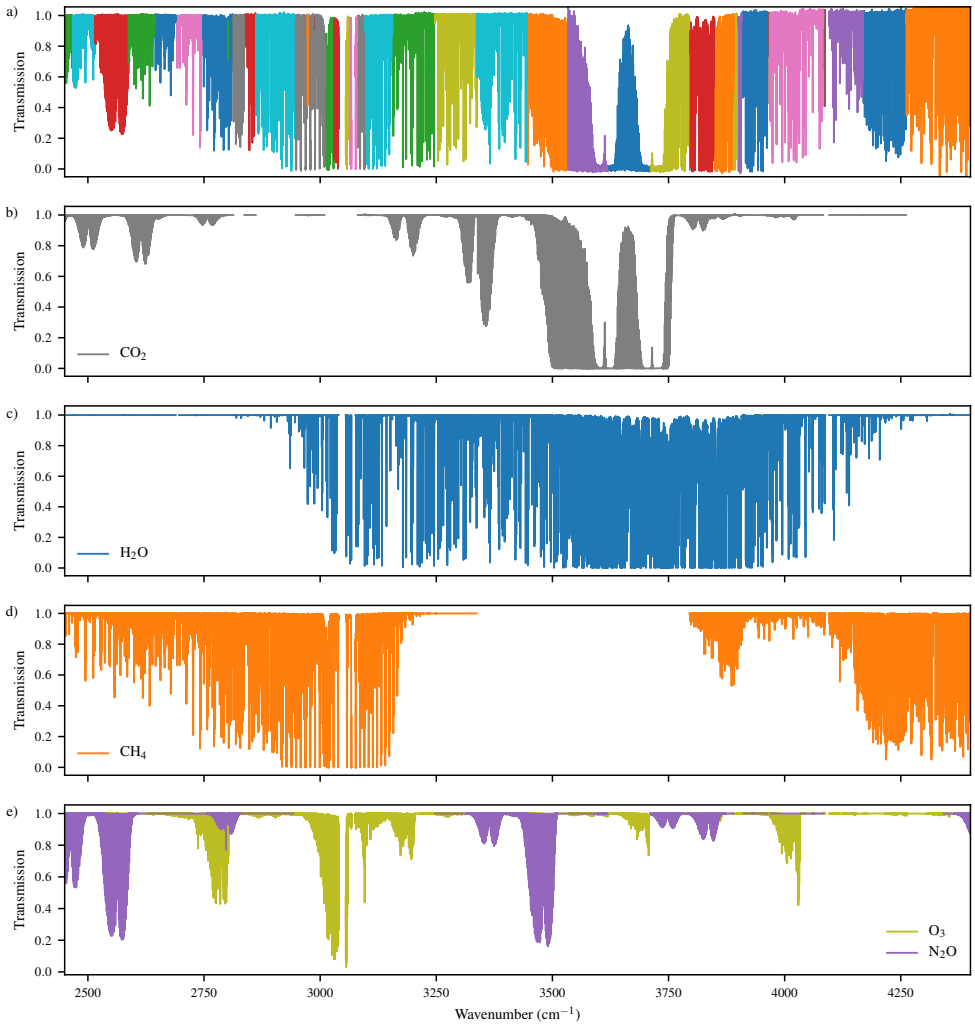

Figure 1: A look at ACE-FTS observations in the ExoMars spectral region of interest: a) mean ACE-FTS spectra at the 0.052 atm pressure level (near 20 km), the colours indicate different fitting windows; b) contributions from CO_2; c) contributions from H_2O; d) contributions from CH_4; e) contributions from O_3 and N_2O.

magnitudes of absorption features due to major gas species in the Earth's

atmosphere: CO_2, H_2O, CH_4, O_3, and N_2O.

5. Results

We begin with an overview of the differences between the HITRAN 2016 and GEISA 2015 line lists in the ExoMars spectral region of interest, 2325–4350 cm^{-1}. Figure 2 shows mean ACE-FTS spectra averaged at three different pressure levels corresponding to approximately 20, 40, and 60 km tangent altitudes. Each primary panel, for each pressure level, shows the mean ACE-FTS spectra, averaged over 125 occultations, for each fitting window (Figure 2 does not show continuous ACE-FTS spectra). Shown over top of the mean ACE-FTS spectra, is the mean of the calculated best fits for each window when using the HITRAN 2016 line list (as an example). It is important to note that the noise level of the ACE-FTS spectra is not constant with wavenumber (Boone et al., 2005), and the noise can be seen increasing towards higher wavenumbers in Figure 2, even after averaging the ACE-FTS spectra.

The secondary panels in Figure 2 show the mean residuals for each fitting window at each pressure level. Shown are mean residuals when fitting with HITRAN 2012, GEISA 2015, and HITRAN 2016. HITRAN 2012 tends to have the largest numbers of errors and both newer line lists improve upon it. The most significant errors are in the CO_2 band centred at 3508 cm^{-1}, which were corrected in the 2016 edition (and not present in GEISA 2015). Difficulty in fitting strong CO_2 lines in the region between 3500–3600 cm^{-1} persists when using all three line lists, but this is also due to a strong increase in detector noise in that region, visible in the mean spectra, especially at the

Table 1: List of spectral fitting windows used to evaluate the HITRAN 2016 and GEISA 2015 line lists with ACE-FTS solar occultation observations of the Earth's atmosphere. Given for each fitting window are: centre wavenumber, window width, and gases fit in the window.

Centre $\tilde{\nu}$ (cm^{-1})	Width (cm^{-1})	Gases fit
2455.5	25.9	CO_2, CH_4, H_2O, N_2O, O_3
2491.5	47.9	CO_2, CH_4, H_2O, N_2O, O_3
2551.55	71.35	H_2O, CO_2, O_3, N_2O, CH_4
2615.74	56.2	CO_2, CH_4, H_2O, N_2O, O_3, HCl, C_2H_6
2666.6	44.76	H_2O, CO_2, O_3, N_2O, CH_4, HCl, C_2H_6
2689.8	0.62	HDO, CO_2, O_3, N_2O, CH_4
2692.76	0.55	HDO, CO_2, O_3, N_2O, CH_4
2708.17	0.54	HDO, CO_2, O_3, N_2O, CH_4
2722.25	52.0	CO_2, CH_4, C_2H_6, H_2O, N_2O, O_3, HCl, HDO
2780.74	65.15	CO_2, CH_4, C_2H_6, H_2O, N_2O, O_3, HCl, HDO
2801.6	0.49	HDO, CO_2, O_3, N_2O, CH_4
2825.0	22.95	H_2O, O_3, N_2O, CH_4, HDO, HCl
2849.15	24.55	HDO, CO_2, H_2O, CH_4, C_2H_6, O_3, N_2O, HCl
2904.43	85.10	H_2O, O_3, N_2O, CH_4, HDO, HCl, NO_2, OCS
2973.65	1.21	C_2H_6, CO_2, H_2O, CH_4, O_3
2978.2	62.0	CO_2, CH_4, C_2H_6, C_2H_4, H_2O, O_3, HCl, HDO
2983.49	0.78	C_2H_6, CO_2, O_3, CH_4
2986.74	0.58	C_2H_6, CO_2, O_3
2989.98	0.80	C_2H_6, CO_2, O_3, CH_4
2993.52	1.23	C_2H_6, CO_2, O_3, CH_4, H_2O
3022.13	18.14	CH_4, H_2O, C_2H_6, C_2H_4, O_3, HCl
3035.08	9.2	CH_4, H_2O, C_2H_6, C_2H_4, O_3
3057.72	5.1	CH_4, H_2O, O_3
3065.86	3.35	CH_4, H_2O, O_3
3077.36	2.54	CH_4, H_2O, O_3

Table 2: List of spectral fitting windows used to evaluate the HITRAN 2016 and GEISA 2015 line lists with ACE-FTS solar occultation observations of the Earth's atmosphere. Given for each fitting window are: centre wavenumber, window width, and gases fit in the window.

Centre $\tilde{\nu}$ (cm^{-1})	Width (cm^{-1})	Gases fit
3089.75	17.5	CH_4, H_2O, C_2H_6, C_2H_4, CO_2, O_3
3126.65	58.0	CO_2, CH_4, C_2H_4, H_2O, O_3, HDO
3202.0	90.0	H_2O, CO_2, CH_4, O_3, HCN
3292.0	90.0	H_2O, CO_2, CH_4, O_3, HCN, N_2O
3391.15	108.6	CO_2, H_2O, C_2H_2, NH_3, HCN, N_2O, O_3, HDO
3489.0	86.0	H_2O, CO_2, O_3, N_2O
3577.0	86.0	H_2O, CO_2, O_3, N_2O, HNO_3, HDO
3665.0	86.0	H_2O, CO_2, O_3, N_2O, HNO_3, HDO
3753.0	86.0	H_2O, CO_2, O_3, N_2O, HF, HDO
3798.8	7.46	H_2O, CO_2, CH_4, O_3
3822.5	51.0	CO_2, H_2O, N_2O, O_3, CH_4, HF, HDO
3869.14	42.0	H_2O, CO_2, O_3, N_2O, CH_4, HF, HDO
3895.36	10.18	H_2O, CO_2, CH_4, O_3
3903.93	6.17	H_2O, CO_2, CH_4, O_3
3936.15	58.0	CO_2, H_2O, N_2O, O_3, CH_4, HF, HDO
3967.79	2.0	H_2O, CO_2, CH_4, O_3
4026.0	114.0	H_2O, CO_2, O_3, N_2O, CH_4, HF, CO
4085.69	3.4	HDO, CO, H_2O, O_3, CH_4
4115.21	5.62	HDO, CO, O_3, CH_4
4128.34	9.53	HDO, CO, H_2O, O_3, CH_4
4132.1	72.5	CO, H_2O, CO_2, CH_4, O_3
4214.2	94.1	CO, H_2O, CO_2, CH_4, O_3
4300.4	76.6	CO, H_2O, CH_4, O_3
4377.0	75.4	H_2O, O_3, CH_4, N_2O, CO
4436.2	42.6	CO_2, H_2O, CH_4

lowest pressure level.

In general, HITRAN 2016 performs better than GEISA 2015, and larger mean residuals are seen in Figure 2. The largest differences are observed the lowest pressure levels, while both line lists perform similarly at higher tangent altitudes. This suggests that the errors are related to either increased pressure and pressure broadening at lower altitudes, or (and) that the magnitude of the errors are related to line depth, and that when the line depths are small, the errors are less than the instrument noise. When CH_4 or CO_2 lines are saturated, the residuals show the negative impact of untreated line mixing, which was not implemented in this spectral region for this study, but is available in GGG (Mendonca et al., 2016). Key areas that GEISA 2015 has difficulty with relative to HITRAN 2016 are between 2700–3200 cm^{-1}, when strong CH_4 lines absorb totally, between 4100–4300 cm^{-1}, where errors are related to O_3 lines and also CH_4 lines (shown in the following section). These are also errors near 3800 cm^{-1} related to H_2O. Fitting the strong CO_2 lines between 3500–3700 cm^{-1} is challenging for GGG using any line list, as shown in Figure 2, especially the middle pressure level. The ν_1 band of HNO_3 is located in this region which is significant at 20 km.

At lower wavenumbers, where detector noise is lowest, there are systematic features observable in the mean residuals when using either line list. Near 2550 cm^{-1}, this is related to line widths in an N_2O absorption band. Near 2650 cm^{-1}, there is an observed absorption band of HNO_3 that is not included in either line list. Several HNO_3 bands are observable in ACE-FTS spectra that are not contained in the HITRAN or GEISA line lists. Weaker bands result in an apparent baseline curvature, while stronger bands show

a distinct vibration-rotation band structure in the residuals. Examples are shown in the following section.

Figure 3 shows the mean RMS for each fitting window, at each pressure level. The RMS was computed for each ACE-FTS occultation in a given window, and shown are the means of the RMS values, with the standard deviation of the mean. At the highest pressure level (top panel, near 60 km), all three line lists perform similarly. In the middle pressure level, near 40 km, we observe strong increases in the mean RMS values, and their uncertainties, where line depths extend beyond 50%, just above 3500 cm^{-1} due to CO_2, and near 3000 cm^{-1} due to CH_4. At the lowest pressure level, the RMS uncertainties increase strongly for all windows, and the differences between line lists become most apparent. At this level, we see deviations between HITRAN 2012 and 2016, at the same locations observed in Figure 2. This analysis also supports the observations made from Figure 2 regarding GEISA 2015. Specific examples and windows are explored in the following section.

6. Specific examples

6.1. 2440 – 2660 cm^{-1}: N_2O and HNO_3

The spectral region between 2440 – 2660 cm^{-1} was covered by four broad fitting windows centred at 2455.5, 2491.5, 2551.55, and 2615.74 cm^{-1}. This region is characterized primarily by the P and R branches of two vibration-rotation bands of N_2O, centred near 2462 and 2562 cm^{-1}, and two vibration-rotation bands of CO_2, centred near 2501 and 2614 cm^{-1}. For these bands, all three spectroscopic line lists perform similarly. In the 2491.5 cm^{-1} window, small, but visible, improvements are apparent where CO_2 lines are present in

the two updated editions of the line lists when compared to HITRAN 2012.

Both the GEISA 2015 and HITRAN 2016 line lists perform almost equivalently in this region. However, there are apparent problems in the fitting, and these problems persist in both data sets. At the lower pressure level, the N_2O fits produce large mean residuals whose shape is indicative of errors in line width. These errors do not persist at the higher pressure levels and are likely due to errors in the broadening parameters in the line lists. The mean ACE-FTS spectra and mean residuals for the 2551.55 cm^{-1} window, which are shown in Figure 4. The lines in this window are mainly due to N_2O, with some CH_4 lines throughout, and the edge of an R branch of CO_2 on the left side.

Figure 5 shows the same information as Figure 4, but for the 2615.74 cm^{-1} window. Again, both the GEISA 2015 and HITRAN 2016 line lists perform equivalently, and, again, there are systematic differences between the observations and the computed spectra. These differences are due to HNO_3 lines not included in either line list. The broad curvature of the baseline in the residuals is due to a weaker band, while the distinct peaks to the right side of Figure 4 are the P branch of a stronger HNO_3 vibration-rotation band. There is a corresponding R branch in the adjacent 2666.6 cm^{-1} window. The feature of another weak HNO_3 band is also present in the 2491.5 cm^{-1} window, and stronger missing lines are seen in the 2978.2 cm^{-1} window, between 2985–3010 cm^{-1}, and in the 3391.15 cm^{-1} window, between 3390–3415 cm^{-1}. That these are due to HNO_3 is verified by measurements made for the line list distributed by the Pacific Northwest National Laboratory (PNNL) (Sharpe et al., 2004; Johnson et al., 2010). Supplementary HNO_3 line lists are used

for ACE-FTS and TCCON retrievals.

6.2. 2660 – 3440 cm^{-1}: CH_4

This wavenumber region is characterized by strong CH_4 absorption features, but also contains important bands of O_3, N_2O and CO_2. This region was covered by several narrow windows and 12 wide windows ranging in width between 18–108 cm^{-1}. The first window centred at 2722.25 cm^{-1} features three strong CH_4 lines, and many associated weaker lines, and there are significant residual errors about each due to unaccounted line mixing. Toon et al. (2016) pointed out a positional error in a CH_4 line at 2742.3 cm^{-1} that was introduced into HITRAN 2012 after the 2008 version. This error is present in GEISA 2015 and HITRAN 2016, and is shown in Figure 6a. While positive changes have been made to the HITRAN 2016 line list, correcting the positional error, strong residual features remain, but these are most likely due to unaccounted line mixing for such strong lines fit at a low altitude. This window also features several weak O_3 lines that are well fit by both line lists, except a small region around 2705–2710 cm^{-1} where fitting with GEISA 2015 results in larger mean residuals than fitting with HITRAN 2016, on the order of 0.005.

The window centred at 2780.74 cm^{-1} contains weaker CH_4 lines and a large O_3 band. Both line lists perform similarly here, but there is what appears to be a single missing line in the GEISA 2015 list. This is an ozone line at 2773.15 cm^{-1} that is not missing, but has an error in line strength, shown in Figure 6b. Toon et al. (2016) pointed out an error in position in an O_3 resonance transition at 2761.42 cm^{-1} that is seen in HITRAN 2012 and GEISA 2015, but has been corrected in HITRAN 2016. However, there are

new O_3 positional errors at 2763.86 and 2798.0 cm^{-1} in the HITRAN 2016 line list that were not present in HITRAN 2012.

The fitting window centred at 2825.0 cm^{-1} presents one of the largest discrepancies between HITRAN 2016 and GEISA 2015. The mean ACE-FTS spectra and mean residuals when fitting with the three line lists are shown in Figure 7 for the lowest pressure level. These discrepancies are characteristic of the strong CH_4 lines throughout this region, and the systematic differentiation between fitting results using the two line lists is seen in Figure 3. There is little difference between the two versions of HITRAN, and both result in mean residual errors on the order of ± 0.01 about strong CH_4 lines. In several positions, however, when fitting with GEISA 2015, these residuals can be twice as large.

Windows centred at 2849.15, 2904.43, 2978.2 cm, and 3126.65^{-1} are similar to those preceding, predominantly featuring strong CH_4 lines, with line mixing errors apparent in the mean residuals when using either line list, but the largest residuals are found when using GEISA 2015. In the 2978.2 cm^{-1} window, there are several saturated (at low altitude) CH_4 lines, and the beginning of a broad, strong band of O_3 lines, but also a set of HNO_3 lines that are missing in both line lists.

The 3022.13 cm^{-1} window contains a mixture of strong O_3 and CH_4 lines. There is an opaque region about 5 cm^{-1} wide at the lower pressure level, which is the Q-branch of this CH_4 band. This feature is critically important for ExoMars, as it is the strongest and broadest CH_4 feature in the available wavenumber range, and where the ExoMars instruments will focus their search for a CH_4 signature. Mean residuals on the right side of

the Q-branch (3018 cm^{-1}) are nearly equivalent when using GEISA 2015 or HITRAN 2016. On the left side (3015 cm^{-1}), mean residuals when using GEISA 2015 are larger than when using HITRAN 2016 by 0.01–0.02. Most of the fitting differences in this region can be attributed to CH_4, but there is also a weaker HCl line at 3014.4 cm^{-1} that contributes to these differences. Note that the residuals for both line lists are significant ($\sim$ 0.002) even at the highest pressure level (near 60 km), where line depths are much weaker and only extend to 0.9. Of particular interest to ExoMars is the recently observed, weak CO_2 band centred near 3000 cm^{-1} that overlaps with these strong CH_4 features (Bertaux et al., 2008; Villanueva et al., 2008). This band is not visible in terrestrial solar occultation observations, its lines are too weak relative to the abundant absorption features of CH_4 and O_3.

Figure 8 shows the mean spectra and mean residuals for fitting window 3089.75 cm^{-1}. This region contains a set of three CH_4 lines near 3090 cm^{-1} that are poorly fit with either line list. When using HITRAN 2012 and HITRAN 2016, the magnitude of the mean residuals is 0.04, which is on the order of the line mixing errors seen when fitting stronger lines. When using GEISA 2015, the mean residuals are 50% larger. Figure 8 also shows a pair of saturated CH_4 lines, and fitting errors characteristic of such lines.

The window centred at 3126.65 cm^{-1} has some of the strongest CH_4 lines, and, therefore, the largest residuals. GEISA 2015 and HITRAN 2016 perform similarly here. The window centred at 3202.0 cm^{-1} contains the right edge of CH_4 ν_2 band. At higher wavenumbers, H_2O absorption becomes dominant. This window also features overlapping CO_2 and O_3 bands, the edge of the strong CH_4 band, and several water vapour lines. The 3292.0 cm^{-1} window

contains H_2O and CO_2 lines, with an H_2O line strength error at 3254.15 cm^{-1} that has been reduced between HITRAN 2012 and HITRAN 2016, but is still significant in both HITRAN 2016 and GEISA 2015. This window contains several other H_2O lines where significant improvements were made to both line lists since HITRAN 2012 (e.g., at 3273.4 and 3276.5 cm^{-1}). The 3391.15 cm^{-1} window is similar, but hosts another set of HNO_3 lines missing from both line lists. There is also an H_2O line strength error at 3367.65 cm^{-1} in both GEISA 2015 and HITRAN 2016 that was not significant in HITRAN 2012.

6.3. 3440 – 3770 cm^{-1}: CO_2

This region was covered by five wide windows centred at 3391.15, 3489.0, 3577.0, 3665.0, and 3753.0 cm^{-1}. These windows cover the strongest CO_2 vibration-rotation bands observed by the ExoMars instruments. Throughout this region, there are only small differences between fits using GEISA 2015 and HITRAN 2016. However, there are significant improvements to several lines throughout since HITRAN 2012. Figure 9 shows the mean spectra and residuals for the window centred at 3489.0 cm^{-1}, where the most dramatic improvement is seen. The spectroscopic parameters for an entire band have been updated, resulting in significant improvements to fitting.

6.4. 3770 – 4080 cm^{-1}: H_2O

This spectral region, covered by four broad fitting windows centred at 3822.5, 3869.14, 3936.15, and 4026.0 cm^{-1}, features the strongest set of water vapour lines in the ExoMars region of interest. It is in this region where we again find that spectral fitting with the HITRAN 2016 results in smaller

residuals than when using GEISA 2015, as seen in Figure 3. Figure 10 shows the window centred at 3869.14 cm^{-1}. The primary features are broad, saturated H_2O lines, but there are also many smaller CH_4 and N_2O lines, and many very weak lines from CO_2 and O_3. The lines where fitting with GEISA 2015 resulted in systematic residual errors are largely attributable to weaker O_3 lines. Similar behaviour is seen in the window centred at 3822.5 cm^{-1}, where several O_3 lines are not contained in GEISA 2015. Note the marked improvement in the strong H_2O line between HITRAN 2012 and the newer line lists near 3886 cm^{-1}, as shown in Figure 6c, but clearly visible in Figure 10.

The two windows at 3936.15 and 4026.0 cm^{-1} show improvements over the previous two windows when comparing GEISA 2015 and HITRAN 2016. The 3936.15 cm^{-1} window contains a portion of an O_3 P-branch. Significant residuals when using GEISA 2015 are from widely spaced CH_4 lines (e.g., at 3912.15, 3914.6, and 3914.9 cm^{-1}), rather than O_3. Two of these features near 3914.6 cm^{-1} are shown in Figure 6d. There is an H_2O line strength error in the HITRAN 2016 line list at 3925.15 cm^{-1} that was not present in HITRAN 2012, nor GEISA 2015. The 4026.0 cm^{-1} window hosts an O_3 band, for which all line lists have difficulty accurately fitting over the region of the Q-branch. The O_3 band in this region is much better characterized by GEISA 2015 than that covered by the 3822.5 and 3869.14 cm^{-1} windows, but there remain small discrepancies in some minor CH_4 lines, especially towards the right edge of the window at 4080.65 and 4082.8 cm^{-1}.

6.5. 4080 – 4420 cm^{-1}: CH_4

Above 4100 cm^{-1}, the ACE-FTS noise increases, as can be seen in Figure 2, and it becomes difficult to evaluate the line lists further. This region is characterized by a decreasing density of H_2O lines, increasingly stronger, and more dense CH_4 absorption features, and a band of broadly spaced CO lines. We evaluated five wide fitting windows in this region centred at 4132.1, 4214.2, 4300.4, 4377.0, and 4436.2 cm^{-1}. At 4115.65 cm^{-1}, a CH_4 line missing in HITRAN 2012, as identified by Toon et al. (2016), was added (also included in GEISA 2015). There are CH_4 line strength errors in the GEISA 2015 line list at 4133.35 cm^{-1} and 4103.2 cm^{-1} that result in mean residuals on the order of 0.1 at lower pressure levels. The latter is also apparent in HITRAN 2016, despite not being present in HITRAN 2012.

As shown in Figure 3, the mean RMS values dramatically increase in this spectral region for all evaluated line lists. At the lowest pressure level, fitting with HITRAN 2016 results in the smallest residuals and the lowest mean RMS values. It must be noted that the magnitude of the difference between results using HITRAN 2016 and GEISA 2015 is on the order of the difference between changing pressure levels, and that is only $\sim 1/5$ of the magnitude of the mean RMS. Therefore, errors due to differences in the spectroscopic parameters are much, much smaller than the noise level of the instrument in this region.

The window centred at 4214.2 cm^{-1} features the most dramatic difference between fitting using GEISA 2015 and fitting using HITRAN 2016. Mean residuals with magnitudes greater than 0.1 come from several CH_4 lines near 4208, 4229, and 4255 cm^{-1}.

7. Conclusions

This study was motivated by the release of two new editions of spectroscopic line lists, the 2015 version of GEISA and the 2016 version of HITRAN, and the launch and arrival of the ExoMars Trace Gas Orbiter as Mars, equipped with two suits of spectroscopic instruments dedicated to characterizing the Martian atmosphere. The largest efforts made recently towards updating infrared spectroscopic databases has been in support of terrestrial greenhouse gas observatories such as OCO-2, GOSAT, and TCCON. Since the Martian atmosphere in composed of 96.5% CO_2, these updates are very significant for the ExoMars mission. Our objective was to validate the two line lists in the range of 2325–4350 cm^{-1} by examining spectral fitting results for terrestrial solar occultation observations made by ACE-FTS.

This work follows that of Toon et al. (2016) who compared different versions of HITRAN, up to the 2012 release, in the spectral range of 670–5620 cm^{-1} using the solar occultation measurements made by the MkIV FTS. They identified several errors in HITRAN 2012, some persisting from previous releases, and others newly introduced. The analysis in Toon et al. (2016) is expanded in Toon (2019), which includes a detailed analysis of HITRAN 2016 using laboratory and solar occultation spectra. Because spectroscopic parameters taken from previous HITRAN versions for some gases in some spectral regions perform better, and because HITRAN may be incomplete in some spectral regions (*e.g.,* HNO_3), the TCCON and GGG development teams maintain a custom line list, as do other spectroscopic analysis teams, such as ACE-FTS.

The 2016 edition of the HITRAN line list addressed several errors identi-

fied in the 2012 edition by Toon et al. (2016), such as the positional error in an O_3 resonance transition at 2761.42 cm^{-1} (still persists in GEISA 2015). We have observed, however, a few minor errors introduced into HITRAN 2016 since the 2012 edition, such as the H_2O line strength errors at 3367.65 cm^{-1} (also in GEISA 2015) and 3925.15 cm^{-1}.

For ExoMars, the gases of primary interest are CO_2, H_2O, CO, and CH_4. Changes to line position and strength have been made to CO_2 lines across our spectral region. For terrestrial spectra, the strongest improvements seen in fitting coincide with the strongest absorption features, and the greatest improvement is seen between 3470–3530 cm^{-1} for both GEISA 2015 and HITRAN 2016. In no region were increased residuals seen for CO_2 lines when using the updated line list editions when compared to HITRAN 2012. In the terrestrial observations, we also observe significant improvements to a subset of H_2O lines, especially at higher wavenumbers, such as near 3093.7 or 3885.5 cm^{-1}. With the exception of individual CH_4 line errors, little difference is observed in the CH_4 or CO transitions in this spectral region between HITRAN 2012 and 2016.

Of key interest to us was the CO_2 vibration-rotation band centred at 2982 cm^{-1} and partially overlapping the critically important CH_4 ν_2 band. When comparing synthetic spectra generated with HITRAN 2016 or GEISA 2015, significant differences in these lines are seen. This band is absent from GEISA 2015, but present in HITRAN 2012 and 2016. The lines included in HITRAN 2016 have significantly increased line strengths relative to HITRAN 2012. Unfortunately, in terrestrial observations, these lines are too weak relative to interfering species, especially CH_4, and noise. It is not observed

in the ACE-FTS spectra examined here above background noise levels, so residuals between spectral fits using HITRAN 2012 and 2016 have not been compared.

A critical difference between the application of spectroscopic calculations for Earth and Mars is that the because the Martian atmosphere is predominantly CO_2 rather than N_2, the collision-induced broadening parameters computed for HITRAN and GEISA will not be applicable to the Martian atmosphere. There is ongoing work to determine spectroscopic parameters for a CO_2-rich atmosphere: *e.g.*, Gamache et al. (2016); Devi et al. (2017) for water vapour; and Li et al. (2015) for CO. However, this study does not attempt to validate these parameters, nor does it evaluate the CO_2 self-broadening parameters.

When comparing the 2015 version of the GEISA line list to the latest, 2016, release of HITRAN, we observe that lower RMS values are found for residuals from the majority of the spectral windows between 2325–4350 cm^{-1} used here. We find that these are primarily due to differences in line strength or position for strong O_3 and CH_4 lines. There are some minor errors in specific lines noted as well.

We were surprised to find a large number of O_3 lines missing from GEISA 2015 in the 3830–3870 cm^{-1} region that were present in HITRAN 2012. The primary source of O_3 lines both HITRAN 2016 and GEISA 2015 is the Spectroscopy and Molecular Properties of Ozone (S&MPO) information system (Babikov et al., 2014) maintained by Reims University and the Institute of Atmospheric Optics (Tomsk). For GEISA 2015, new measurements of lines around this region were made at Reims University by Barbe

et al. (1997, 2012), but those lines precisely between 3830–3870 cm^{-1} are attributed to a private communication from Barbe (2011). O_3 line parameters in HITRAN 2016 are also included in the S&MPO database. In the region 3623–4229 cm^{-1}, HITRAN also includes an updated hot band from Barbe et al. (2013).

Our analysis fit the hydrogen halides HCl (between 2600–3050 cm^{-1}) and HF (between 3700–4100 cm^{-1}). Parameters for these gases were not updated in the 2011 or 2015 editions of GEISA, but new calculations were implemented in the 2012 edition of HITRAN (Li et al., 2013). The result is differences in line position when performing spectral fitting with HITRAN 2016 or GEISA 2015. Mean differences are very small relative to the noise of the ACE-FTS observations, less than 1%, with HITRAN 2016 performing slightly better at these line locations (*e.g.*, 2925.9 cm^{-1} or 2944.93 cm^{-1} for HCl, and 3877.7 cm^{-1} or 3920.3 cm^{-1} for HF).

In conclusion, we have noted consistent improvement in both line lists since HITRAN 2012, have noted errors and deficiencies in both line lists where found, and we hope that the collaborations in charge of both line lists will find this analysis useful when compiling the next release. However, for the purposes of the ExoMars TGO ACS and NOMAD instruments, we recommend HITRAN 2016 for use. HITRAN 2016 shows marked improvement over HITRAN 2012 in CO_2 and H_2O transitions (as does GEISA 2015). GEISA 2015 currently produces larger residuals for strong CH_4 lines that are critical for ExoMars, while an important CO_2 band centred at 2982 cm^{-1} has not yet been introduced.

8. Acknowledgements

All spectral fitting was performed by KSO using the GGG software suite. The ACE-FTS spectra were provided by CDB, who also provided valuable input towards their use and fitting. The GGG software suite is maintained by GCT at JPL (tccon-wiki.caltech.edu). Input on interpreting the results and the spectroscopy in the target region was provided by CDB and GCT. The HITRAN line list is hosted by the Harvard-Smithsonian Center for Astrophysics under the continued direction of Dr Laurence S. Rothman (hitran.org). The GEISA line list is compiled by the Atmospheric Radiation Analysis group at LMD and hosted by the Institut Pierre Simon Laplace (cds-espri.ipsl.upmc.fr/GEISA/geisa_raie_2015.php). Tools hosted by the Earth Observation Data Group were used to reformat the GEISA 2015 line list into the format of the HITRAN line list (eodg.atm.ox.ac.uk/RFM/geihit.html). This work was performed in support of the ExoMars TGO ACS instrument and funded by the National Centre for Space Studies of France (CNES) and the Natural Sciences and Engineering Research Council of Canada (NSERC) (PDF - 516895 - 2018).

References

Armante, R., Scott, N., Crevoisier, C., Capelle, V., Crepeau, L., Jacquinet, N., Chédin, A., Sep. 2016. Evaluation of spectroscopic databases through radiative transfer simulations compared to observations. Application to the validation of GEISA 2015 with IASI and TCCON. J. Mol. Spectrosc. 327, 180–192.

637 Babikov, Y. L., Mikhailenko, S. N., Barbe, A., Tyuterev, V. G., Sep. 2014.
638 S&MPO - An information system for ozone spectroscopy on the WEB. J.
639 Quant. Spectrosc. Radiat. Transfer 145, 169–196.

640 Bailey, J., Jun. 2009. A comparison of water vapor line parameters for mod-
641 eling the Venus deep atmosphere. Icarus 201, 444–453.

642 Barbe, A., De Backer, M.-R., Starikova, E., Tashkun, S. A., Thomas, X.,
643 Tyuterev, V. G., Jul. 2012. FTS high resolution spectra of $^{16}O_3$ in 3500
644 and 5500 cm^{-1} regions. First example of new theoretical modelling for a
645 polyad of strongly coupled states. J. Quant. Spectrosc. Radiat. Transfer
646 113, 829–839.

647 Barbe, A., Mikhailenko, S., Starikova, E., De Backer, M.-R., Tyuterev,
648 V. G., Mondelain, D., Kassi, S., Campargue, A., Janssen, C., Tashkun, S.,
649 Kochanov, R., Gamache, R., Orphal, J., Nov. 2013. Ozone spectroscopy in
650 the electronic ground state: High-resolution spectra analyses and update
651 of line parameters since 2003. J. Quant. Spectrosc. Radiat. Transfer 130,
652 172–190.

653 Barbe, A., Plateaux, J. J., Mikhailenko, S., Tyuterev, V. G., Oct. 1997.
654 Infrared Spectrum of Ozone in the 4600 and 5300 cm $^{-1}$Regions: High
655 Order Accidental Resonances through the Analysis of $\nu_1 + 2\nu_2 + 3\nu_3 - \nu_2$, $\nu_1 + 2\nu_2 + 3\nu_3$, and $4\nu_1 + \nu_3$Bands. J. Mol. Spectrosc. 185, 408–416.

657 Barber, R. J., Tennyson, J., Harris, G. J., Tolchenov, R. N., May 2006. A
658 high-accuracy computed water line list. Mon. Not. R. Astron. Soc. 368,
659 1087–1094.

Bernath, P. F., McElroy, C. T., Abrams, M. C., Boone, C. D., Butler, M., Camy-Peyret, C., Carleer, M., Clerbaux, C., Coheur, P.-F., Colin, R., DeCola, P., DeMazière, M., Drummond, J. R., Dufour, D., Evans, W. F. J., Fast, H., Fussen, D., Gilbert, K., Jennings, D. E., Llewellyn, E. J., Lowe, R. P., Mahieu, E., McConnell, J. C., McHugh, M., McLeod, S. D., Michaud, R., Midwinter, C., Nassar, R., Nichitiu, F., Nowlan, C., Rinsland, C. P., Rochon, Y. J., Rowlands, N., Semeniuk, K., Simon, P., Skelton, R., Sloan, J. J., Soucy, M.-A., Strong, K., Tremblay, P., Turnbull, D., Walker, K. A., Walkty, I., Wardle, D. A., Wehrle, V., Zander, R., Zou, J., Jun. 2005. Atmospheric Chemistry Experiment (ACE): Mission overview. Geophys. Res. Lett. 32, L15S01.

Bertaux, J.-L., Vandaele, A. C., Wilquet, V., Montmessin, F., Dahoo, R., Villard, E., Korablev, O., Fedorova, A., May 2008. First observation of 628 CO_2 isotopologue band at 3.3 μm in the atmosphere of Venus by solar occultation from Venus Express. Icarus 195, 28–33.

Birk, M., Wagner, G., Loos, J., Lodi, L., Polyansky, O. L., Kyuberis, A. A., Zobov, N. F., Tennyson, J., Dec. 2017. Accurate line intensities for water transitions in the infrared: Comparison of theory and experiment. J. Quant. Spectrosc. Radiat. Transfer 203, 88–102.

Boone, C. D., Nassar, R., Walker, K. A., Rochon, Y., McLeod, S. D., Rinsland, C. P., Bernath, P. F., Nov. 2005. Retrievals for the atmospheric chemistry experiment Fourier-transform spectrometer. Appl. Opt. 44, 7218–7231.

683 Brown, L. R., Sung, K., Benner, D. C., Devi, V. M., Boudon, V., Gabard,
684 T., Wenger, C., Campargue, A., Leshchishina, O., Kassi, S., Monde-
685 lain, D., Wang, L., Daumont, L., Régalia, L., Rey, M., Thomas, X.,
686 Tyuterev, V. G., Lyulin, O. M., Nikitin, A. V., Niederer, H. M., Albert,
687 S., Bauerecker, S., Quack, M., O'Brien, J. J., Gordon, I. E., Rothman,
688 L. S., Sasada, H., Coustenis, A., Smith, M. A. H., Carrington, T., Wang,
689 X.-G., Mantz, A. W., Spickler, P. T., Nov. 2013. Methane line parameters
690 in the HITRAN2012 database. J. Quant. Spectrosc. Radiat. Transfer 130,
691 201–219.

692 Chédin, A., Husson, N., Scott, N. A., Feb. 1982. GEISA - a Data Base for
693 the Study of Phenomena of Radiative Transfer in Planetary Atmospheres.
694 Bulletin d'Information du Centre de Donnees Stellaires 22, 121.

695 Clarke, J. T., Mayyasi, M., Bhattacharyya, D., Schneider, N. M., McClin-
696 tock, W. E., Deighan, J. I., Stewart, A. I. F., Chaufray, J.-Y., Chaffin,
697 M. S., Jain, S. K., Stiepen, A., Crismani, M., Holsclaw, G. M., Montmessin,
698 F., Jakosky, B. M., Feb. 2017. Variability of D and H in the Martian upper
699 atmosphere observed with the MAVEN IUVS echelle channel. J. Geophys.
700 Res. 122, 2336–2344.

701 Clerbaux, C., Boynard, A., Clarisse, L., George, M., Hadji-Lazaro, J.,
702 Herbin, H., Hurtmans, D., Pommier, M., Razavi, A., Turquety, S., We-
703 spes, C., Coheur, P.-F., Aug. 2009. Monitoring of atmospheric composition
704 using the thermal infrared IASI/MetOp sounder. Atmos. Chem. Phys. 9,
705 6041–6054.

Coudert, L. H., Chelin, P., Aug. 2016. Line position and line intensity analyses of the high-resolution spectrum of $H_2{}^{18}O$ up to the First Triad and J = 17. J. Mol. Spectrosc. 326, 130–135.

Coudert, L. H., Martin-Drumel, M.-A., Pirali, O., Sep. 2014. Analysis of the high-resolution water spectrum up to the Second Triad and to J = 30. J. Mol. Spectrosc. 303, 36–41.

Crisp, D., Atlas, R. M., Breon, F.-M., Brown, L. R., Burrows, J. P., Ciais, P., Connor, B. J., Doney, S. C., Fung, I. Y., Jacob, D. J., Miller, C. E., O'Brien, D., Pawson, S., Randerson, J. T., Rayner, P., Salawitch, R. J., Sander, S. P., Sen, B., Stephens, G. L., Tans, P. P., Toon, G. C., Wennberg, P. O., Wofsy, S. C., Yung, Y. L., Kuang, Z., Chudasama, B., Sprague, G., Weiss, B., Pollock, R., Kenyon, D., Schroll, S., Jan. 2004. The Orbiting Carbon Observatory (OCO) mission. Adv. Space Res. 34, 700–709.

Crisp, D., Pollock, H. R., Rosenberg, R., Chapsky, L., Lee, R. A. M., Oyafuso, F. A., Frankenberg, C., O'Dell, C. W., Bruegge, C. J., Doran, G. B., Eldering, A., Fisher, B. M., Fu, D., Gunson, M. R., Mandrake, L., Osterman, G. B., Schwandner, F. M., Sun, K., Taylor, T. E., Wennberg, P. O., Wunch, D., Jan. 2017. The on-orbit performance of the Orbiting Carbon Observatory-2 (OCO-2) instrument and its radiometrically calibrated products. Atmos. Meas. Tech. 10, 59–81.

Devi, V. M., Benner, D. C., Sung, K., Crawford, T. J., Gamache, R. R., Renaud, C. L., Smith, M. A. H., Mantz, A. W., Villanueva, G. L., Dec. 2017. Line parameters for CO_2- and self-broadening in the ν_3 band of $HD^{16}O$. J. Quant. Spectrosc. Radiat. Transfer 203, 158–174.

730 Durry, G., Li, J. S., Vinogradov, I., Titov, A., Joly, L., Cousin, J., Decarpen-
731 terie, T., Amarouche, N., Liu, X., Parvitte, B., Korablev, O., Gerasimov,
732 M., Zéninari, V., Apr. 2010. Near infrared diode laser spectroscopy of
733 C_2H_2, H_2O, CO_2 and their isotopologues and the application to TDLAS, a
734 tunable diode laser spectrometer for the martian PHOBOS-GRUNT space
735 mission. Appl. Phys. B 99, 339–351.

736 Encrenaz, T., DeWitt, C., Richter, M. J., Greathouse, T. K., Fouchet, T.,
737 Montmessin, F., Lefèvre, F., Bézard, B., Atreya, S. K., Aoki, S., Sagawa,
738 H., May 2018. New measurements of D/H on Mars using EXES aboard
739 SOFIA. Astron. Astrophys. 612, A112.

740 Formisano, V., Atreya, S., Encrenaz, T., Ignatiev, N., Giuranna, M., Dec.
741 2004. Detection of Methane in the Atmosphere of Mars. Science 306, 1758–
742 1761.

743 Gamache, R. R., Farese, M., Renaud, C. L., Aug. 2016. A spectral line list
744 for water isotopologues in the 1100-4100 cm^{-1} region for application to
745 CO_2-rich planetary atmospheres. J. Mol. Spectrosc. 326, 144–150.

746 Giuranna, M., Viscardy, S., Daerden, F., Neary, L., Etiope, G., Oehler,
747 D., Formisano, V., Aronica, A., Wolkenberg, P.and Aoki, S., Cardesn-
748 Moinelo, A., Marn-Yaseli de la Parra, J., Merritt, D., Amoroso, M., 2019.
749 Independent confirmation of a methane spike on Mars and a source region
750 east of Gale Crater. Nat. Geosci., 1752–0908.

751 Gordon, I. E., Rothman, L. S., Hill, C., Kochanov, R. V., Tan, Y., Bernath,
752 P. F., Birk, M., Boudon, V., Campargue, A., Chance, K. V., Drouin, B. J.,

753 Flaud, J.-M., Gamache, R. R., Hodges, J. T., Jacquemart, D., Perevalov,
754 V. I., Perrin, A., Shine, K. P., Smith, M.-A. H., Tennyson, J., Toon,
755 G. C., Tran, H., Tyuterev, V. G., Barbe, A., Császár, A. G., Devi, V. M.,
756 Furtenbacher, T., Harrison, J. J., Hartmann, J.-M., Jolly, A., Johnson,
757 T. J., Karman, T., Kleiner, I., Kyuberis, A. A., Loos, J., Lyulin, O. M.,
758 Massie, S. T., Mikhailenko, S. N., Moazzen-Ahmadi, N., Müller, H. S. P.,
759 Naumenko, O. V., Nikitin, A. V., Polyansky, O. L., Rey, M., Rotger, M.,
760 Sharpe, S. W., Sung, K., Starikova, E., Tashkun, S. A., Auwera, J. V.,
761 Wagner, G., Wilzewski, J., Wcisło, P., Yu, S., Zak, E. J., Dec. 2017.
762 The HITRAN2016 molecular spectroscopic database. J. Quant. Spectrosc.
763 Radiat. Transfer 203, 3–69.

764 Huang, X., Gamache, R. R., Freedman, R. S., Schwenke, D. W., Lee, T. J.,
765 Nov. 2014. Reliable infrared line lists for 13 CO_2 isotopologues up to
766 E′=18,000 cm^{-1} and 1500 K, with line shape parameters. J. Quant. Spec-
767 trosc. Radiat. Transfer 147, 134–144.

768 Irion, F. W., Gunson, M. R., Toon, G. C., Chang, A. Y., Eldering, A.,
769 Mahieu, E., Manney, G. L., Michelsen, H. A., Moyer, E. J., Newchurch,
770 M. J., Osterman, G. B., Rinsland, C. P., Salawitch, R. J., Sen, B., Yung,
771 Y. L., Zander, R., Nov. 2002. Atmospheric Trace Molecule Spectroscopy
772 (ATMOS) Experiment Version 3 data retrievals. Appl. Opt. 41, 6968–6979.

773 Jacquemart, D., Gueye, F., Lyulin, O. M., Karlovets, E. V., Baron, D.,
774 Perevalov, V. I., Jul. 2012. Infrared spectroscopy of CO_2 isotopologues
775 from 2200 to 7000 cm^{-1}: I-Characterizing experimental uncertainties of

positions and intensities. J. Quant. Spectrosc. Radiat. Transfer 113, 961–975.

Jacquinet-Husson, N., Armante, R., Scott, N. A., Chédin, A., Crépeau, L., Boutammine, C., Bouhdaoui, A., Crevoisier, C., Capelle, V., Boonne, C., Poulet-Crovisier, N., Barbe, A., Chris Benner, D., Boudon, V., Brown, L. R., Buldyreva, J., Campargue, A., Coudert, L. H., Devi, V. M., Down, M. J., Drouin, B. J., Fayt, A., Fittschen, C., Flaud, J.-M., Gamache, R. R., Harrison, J. J., Hill, C., Hodnebrog, Ø., Hu, S.-M., Jacquemart, D., Jolly, A., Jiménez, E., Lavrentieva, N. N., Liu, A.-W., Lodi, L., Lyulin, O. M., Massie, S. T., Mikhailenko, S., Müller, H. S. P., Naumenko, O. V., Nikitin, A., Nielsen, C. J., Orphal, J., Perevalov, V. I., Perrin, A., Polovtseva, E., Predoi-Cross, A., Rotger, M., Ruth, A. A., Yu, S. S., Sung, K., Tashkun, S. A., Tennyson, J., Tyuterev, V. G., Vander Auwera, J., Voronin, B. A., Makie, A., Sep. 2016. The 2015 edition of the GEISA spectroscopic database. J. Mol. Spectrosc. 327, 31–72.

Johnson, T. J., Profeta, L. T. M., Sams, R. L., Griffith, D. W. T., Yokelson, R. L., May 2010. An infrared spectral database for detection of gases emitted by biomass burning. Vib. Spectrosc. 53, 97–102.

Kalnay, E., Kanamitsu, M., Kistler, R., Collins, W., Deaven, D., Gandin, L., Iredell, M., Saha, S., White, G., Woollen, J., Zhu, Y., Leetmaa, A., Reynolds, B., Chelliah, M., Ebisuzaki, W., Higgins, W., Janowiak, J., Mo, K. C., Ropelewski, C., Wang, J., Jenne, R., Joseph, D., Mar. 1996. The NCEP/NCAR 40-Year Reanalysis Project. Bull. Am. Astron. Soc. 77, 437–472.

Korablev, O., Montmessin, F., Trokhimovskiy, A., Fedorova, A. A., Shakun, A. V., Grigoriev, A. V., Moshkin, B. E., Ignatiev, N. I., Forget, F., Lefèvre, F., Anufreychik, K., Dzuban, I., Ivanov, Y. S., Kalinnikov, Y. K., Kozlova, T. O., Kungurov, A., Makarov, V., Martynovich, F., Maslov, I., Merzlyakov, D., Moiseev, P. P., Nikolskiy, Y., Patrakeev, A., Patsaev, D., Santos-Skripko, A., Sazonov, O., Semena, N., Semenov, A., Shashkin, V., Sidorov, A., Stepanov, A. V., Stupin, I., Timonin, D., Titov, A. Y., Viktorov, A., Zharkov, A., Altieri, F., Arnold, G., Belyaev, D. A., Bertaux, J. L., Betsis, D. S., Duxbury, N., Encrenaz, T., Fouchet, T., Gérard, J.-C., Grassi, D., Guerlet, S., Hartogh, P., Kasaba, Y., Khatuntsev, I., Krasnopolsky, V. A., Kuzmin, R. O., Lellouch, E., Lopez-Valverde, M. A., Luginin, M., Määttänen, A., Marcq, E., Martin Torres, J., Medvedev, A. S., Millour, E., Olsen, K. S., Patel, M. R., Quantin-Nataf, C., Rodin, A. V., Shematovich, V. I., Thomas, I., Thomas, N., Vazquez, L., Vincendon, M., Wilquet, V., Wilson, C. F., Zasova, L. V., Zelenyi, L. M., Zorzano, M. P., Feb. 2018. The Atmospheric Chemistry Suite (ACS) of Three Spectrometers for the ExoMars 2016 Trace Gas Orbiter. Space Sci. Rev. 214, 7.

Korablev, O., Vandaele, A. C., Montmessin, F., Fedorova, A. A., Trokhimovskiy, A., Forget, F., Lefévre, F., Daerden, F., Thomas, I. R., Trompet, L., Erwin, J. T., Aoki, S., Robert, S., Neary, L., Viscardy, S., Grigoriev, A., Ignatiev, N., Shakun, A., Patrakeev, A., Belyaev, D., Bertaux, J.-L., Olsen, K. S., Baggio, L., Alday, J., Ivanov, Y. S., Bojan, R., et al., 2019. No detection of methane on Mars from early ExoMars Trace Gas Orbiter observations. Nature.

825 Krasnopolsky, V. A., Sep. 2015. Variations of the HDO/H_2O ratio in the
826 martian atmosphere and loss of water from Mars. Icarus 257, 377–386.

827 Krasnopolsky, V. A., Maillard, J. P., Owen, T. C., Dec. 2004. Detection of
828 methane in the Martian atmosphere: evidence for life? Icarus 172, 537–
829 547.

830 Li, G., Gordon, I. E., Hajigeorgiou, P. G., Coxon, J. A., Rothman, L. S.,
831 Nov 2013. Reference spectroscopic data for hydrogen halides, Part II: The
832 line lists. J. Quant. Spectrosc. Radiat. Transfer 130, 284–295.

833 Li, G., Gordon, I. E., Rothman, L. S., Tan, Y., Hu, S.-M., Kassi, S., Cam-
834 pargue, A., Medvedev, E. S., Jan. 2015. Rovibrational Line Lists for Nine
835 Isotopologues of the CO Molecule in the X $^1\Sigma^+$ Ground Electronic State.
836 Astrophys. J. Suppl. Ser. 216, 15.

837 Lodi, L., Tennyson, J., Jul. 2012. Line lists for $H_2{}^{18}O$ and $H_2{}^{17}O$ based
838 on empirical line positions and ab initio intensities. J. Quant. Spectrosc.
839 Radiat. Transfer 113, 850–858.

840 Lodi, L., Tennyson, J., Polyansky, O. L., Jul. 2011. A global, high accuracy
841 ab initio dipole moment surface for the electronic ground state of the water
842 molecule. J. Chem. Phys. 135 (3), 034113–034113.

843 Loos, J., Birk, M., Wagner, G., Dec. 2017a. Measurement of air-broadening
844 line shape parameters and temperature dependence parameters of H_2O
845 lines in the spectral ranges 1850-2280 cm^{-1} and 2390-4000 cm^{-1}. J. Quant.
846 Spectrosc. Radiat. Transfer 203, 103–118.

Loos, J., Birk, M., Wagner, G., Dec. 2017b. Measurement of positions, intensities and self-broadening line shape parameters of H_2O lines in the spectral ranges 1850-2280 cm^{-1} and 2390-4000 cm^{-1}. J. Quant. Spectrosc. Radiat. Transfer 203, 119–132.

Lyulin, O. M., Karlovets, E. V., Jacquemart, D., Lu, Y., Liu, A. W., Perevalov, V. I., Nov. 2012. Infrared spectroscopy of 17O- and 18O-enriched carbon dioxide in the 1700-8300cm-1 wavenumber region. J. Quant. Spectrosc. Radiat. Transfer 113, 2167–2181.

McClatchey, R. A., Benedict, W. S., Clough, S. A., Burch, D. E., Calfee, R. F., Fox, K., Rothman, L. S., Garing, J. S., 1973. AFCRL atmospheric absorption line parameters compilation. Air Force Cambridge Research Laboratories, Bedford, Ma.

Mendonca, J., Strong, K., Toon, G. C., Wunch, D., Sung, K., Deutscher, N. M., Griffith, D. W. T., Franklin, J. E., May 2016. Improving atmospheric CO_2 retrievals using line mixing and speed-dependence when fitting high-resolution ground-based solar spectra. J. Mol. Spectrosc. 323, 15–27.

Mumma, M. J., Villanueva, G. L., Novak, R. E., Hewagama, T., Bonev, B. P., DiSanti, M. A., Mandell, A. M., Smith, M. D., Feb. 2009. Strong Release of Methane on Mars in Northern Summer 2003. Science 323, 1041–1045.

Niederer, H.-M., Wang, X.-G., Carrington, T., Albert, S., Bauerecker, S., Boudon, V., Quack, M., Sep. 2013. Analysis of the rovibrational spectrum of $^{13}CH_4$ in the Octad range. J. Mol. Spectrosc. 291, 33–47.

Nikitin, A. V., Boudon, V., Wenger, C., Albert, S., Brown, L. R., Bauerecker, S., Quack, M., 2013. High resolution spectroscopy and the first global analysis of the Tetradecad region of methane 12CH4. Phys. Chem. Chem. Phys. 15, 10071.

Norton, R. H., Rinsland, C. P., Feb. 1991. ATMOS data processing and science analysis methods. Appl. Opt. 30, 389–400.

Olsen, K. S., Toon, G. C., Boone, C. D., Strong, K., 2015. New temperature and pressure retrieval algorithm for high-resolution infrared solar occultation spectrometry: analysis and validation against ACE-FTS and COSMIC. Atmos. Meas. Tech. Disc. 8, 10823–10873.

Rothman, L. S., Gamache, R. R., Tipping, R. H., Rinsland, C. P., Smith, M. A. H., Benner, D. C., Devi, V. M., Flaud, J.-M., Camy-Peyret, C., Perrin, A., 1992. The HITRAN molecular data base - Editions of 1991 and 1992. J. Quant. Spectrosc. Radiat. Transfer 48, 469–507.

Rothman, L. S., Gordon, I. E., Babikov, Y., Barbe, A., Chris Benner, D., Bernath, P. F., Birk, M., Bizzocchi, L., Boudon, V., Brown, L. R., Campargue, A., Chance, K., Cohen, E. A., Coudert, L. H., Devi, V. M., Drouin, B. J., Fayt, A., Flaud, J.-M., Gamache, R. R., Harrison, J. J., Hartmann, J.-M., Hill, C., Hodges, J. T., Jacquemart, D., Jolly, A., Lamouroux, J., Le Roy, R. J., Li, G., Long, D. A., Lyulin, O. M., Mackie, C. J., Massie, S. T., Mikhailenko, S., Müller, H. S. P., Naumenko, O. V., Nikitin, A. V., Orphal, J., Perevalov, V., Perrin, A., Polovtseva, E. R., Richard, C., Smith, M. A. H., Starikova, E., Sung, K., Tashkun, S., Tennyson, J., Toon, G. C.,

Tyuterev, V. G., Wagner, G., Nov. 2013. The HITRAN2012 molecular spectroscopic database. J. Quant. Spectrosc. Radiat. Transfer 130, 4–50.

Rothman, L. S., Gordon, I. E., Barbe, A., Benner, D. C., Bernath, P. F., Birk, M., Boudon, V., Brown, L. R., Campargue, A., Champion, J.-P., Chance, K., Coudert, L. H., Dana, V., Devi, V. M., Fally, S., Flaud, J.-M., Gamache, R. R., Goldman, A., Jacquemart, D., Kleiner, I., Lacome, N., Lafferty, W. J., Mandin, J.-Y., Massie, S. T., Mikhailenko, S. N., Miller, C. E., Moazzen-Ahmadi, N., Naumenko, O. V., Nikitin, A. V., Orphal, J., Perevalov, V. I., Perrin, A., Predoi-Cross, A., Rinsland, C. P., Rotger, M., Šimečková, M., Smith, M. A. H., Sung, K., Tashkun, S. A., Tennyson, J., Toth, R. A., Vandaele, A. C., Vander Auwera, J., Jun. 2009. The HITRAN 2008 molecular spectroscopic database. J. Quant. Spectrosc. Radiat. Transfer 110, 533–572.

Sen, B., Toon, G. C., Blavier, J.-F., Fleming, E. L., Jackman, C. H., Apr. 1996. Balloon-borne observations of midlatitude fluorine abundance. J. Geophys. Res. 101, 9045–9054.

Sharpe, S. W., Johnson, T. J., Sams, R. L., Chu, P. M., Rhoderick, G. C., Johnson, P. A., Dec. 2004. Gas-Phase Databases for Quantitative Infrared Spectroscopy. Appl. Spectrosc. 58, 1452–1461.

Tashkun, S. A., Perevalov, V. I., Gamache, R. R., Lamouroux, J., Feb. 2015. CDSD-296, high resolution carbon dioxide spectroscopic databank: Version for atmospheric applications. J. Quant. Spectrosc. Radiat. Transfer 152, 45–73.

Tennyson, J., Bernath, P. F., Brown, L. R., Campargue, A., Carleer, M. R., Császár, A. G., Gamache, R. R., Hodges, J. T., Jenouvrier, A., Naumenko, O. V., Polyansky, O. L., Rothman, L. S., Toth, R. A., Carine Vandaele, A., Zobov, N. F., Daumont, L., Fazliev, A. Z., Furtenbacher, T., Gordon, I. E., Mikhailenko, S. N., Shirin, S. V., Jun. 2009. IUPAC critical evaluation of the rotational-vibrational spectra of water vapor. Part I–Energy levels and transition wavenumbers for $H_2{}^{17}O$ and $H_2{}^{18}O$. J. Quant. Spectrosc. Radiat. Transfer 110, 573–596.

Toon, G., 2019. CO_2 Spectroscopy Evaluation: 670 to 7000 cm^{-1}. Tech. rep., Jet Propulsion Laboratory.
URL mark4sun.jpl.nasa.gov/toon/atm18/NDACC_TCCON_2019_Toon-compressed.pdf

Toon, G. C., Oct. 1991. The JPL MkIV interferometer. Opt. Photonics News 2, 19–21.

Toon, G. C., Blavier, J.-F., Sung, K., Rothman, L. S., E. Gordon, I., Oct. 2016. HITRAN spectroscopy evaluation using solar occultation FTIR spectra. J. Quant. Spectrosc. Radiat. Transfer 182, 324–336.

Toth, R. A., Brown, L. R., Miller, C. E., Malathy Devi, V., Benner, D. C., Apr. 2008a. Spectroscopic database of CO_2 line parameters: 4300 7000 cm^{-1}. J. Quant. Spectrosc. Radiat. Transfer 109, 906–921.

Toth, R. A., Miller, C. E., Brown, L. R., Devi, V. M., Benner, D. C., May 2007. Line positions and strengths of ^{16}O ^{12}C ^{18}O, ^{18}O ^{12}C ^{18}O and ^{17}O ^{12}C ^{18}O between 2200 and 7000 cm $^{-1}$. J. Mol. Spectrosc. 243, 43–61.

939 Toth, R. A., Miller, C. E., Brown, L. R., Devi, V. M., Benner, D. C., Sep.
940 2008b. Line strengths of ^{16}O ^{13}C ^{16}O, ^{16}O ^{13}C ^{18}O, ^{16}O ^{13}C ^{17}O and ^{18}O
941 ^{13}C ^{18}O between 2200 and 6800 cm $^{-1}$. J. Mol. Spectrosc. 251, 64–89.

942 Tyuterev, V., Tashkun, S., Rey, M., Kochanov, R., Nikitin, A., Delahaye, T.,
943 Dec. 2013. Accurate Spectroscopic Models for Methane Polyads Derived
944 from a Potential Energy Surface Using High-Order Contact Transforma-
945 tions. J. Phys. Chem. A 117, 13779–13805.

946 Vandaele, A. C., Lopez-Moreno, J.-J., Patel, M. R., Bellucci, G., Daer-
947 den, F., Ristic, B., Robert, S., Thomas, I. R., Wilquet, V., Allen, M.,
948 Alonso-Rodrigo, G., Altieri, F., Aoki, S., Bolsée, D., Clancy, T., Cloutis,
949 E., Depiesse, C., Drummond, R., Fedorova, A., Formisano, V., Funke,
950 B., González-Galindo, F., Geminale, A., Gérard, J.-C., Giuranna, M.,
951 Hetey, L., Ignatiev, N., Kaminski, J., Karatekin, O., Kasaba, Y., Leese,
952 M., Lefèvre, F., Lewis, S. R., López-Puertas, M., López-Valverde, M.,
953 Mahieux, A., Mason, J., McConnell, J., Mumma, M., Neary, L., Neefs,
954 E., Renotte, E., Rodriguez-Gomez, J., Sindoni, G., Smith, M., Stiepen,
955 A., Trokhimovsky, A., Vander Auwera, J., Villanueva, G., Viscardy, S.,
956 Whiteway, J., Willame, Y., Wolff, M., Aug. 2018. NOMAD, an Integrated
957 Suite of Three Spectrometers for the ExoMars Trace Gas Mission: Techni-
958 cal Description, Science Objectives and Expected Performance. Space Sci.
959 Rev. 214, 80.

960 Vandaele, A. C., Neefs, E., Drummond, R., Thomas, I. R., Daerden, F.,
961 Lopez-Moreno, J.-J., Rodriguez, J., Patel, M. R., Bellucci, G., Allen, M.,
962 Altieri, F., Bolsée, D., Clancy, T., Delanoye, S., Depiesse, C., Cloutis, E.,

963 Fedorova, A., Formisano, V., Funke, B., Fussen, D., Geminale, A., Gérard,
964 J.-C., Giuranna, M., Ignatiev, N., Kaminski, J., Karatekin, O., Lefèvre,
965 F., López-Puertas, M., López-Valverde, M., Mahieux, A., McConnell, J.,
966 Mumma, M., Neary, L., Renotte, E., Ristic, B., Robert, S., Smith, M.,
967 Trokhimovsky, S., Vander Auwera, J., Villanueva, G., Whiteway, J., Wil-
968 quet, V., Wolff, M., Dec. 2015. Science objectives and performances of
969 NOMAD, a spectrometer suite for the ExoMars TGO mission. Planet.
970 Space Sci. 119, 233–249.

971 Villanueva, G. L., Mumma, M. J., Novak, R. E., Hewagama, T., May 2008.
972 Identification of a new band system of isotopic CO $_2$ near 3.3 μm: Impli-
973 cations for remote sensing of biomarker gases on Mars. Icarus 195, 34–44.

974 Webster, C. R., Mahaffy, P. R., Atreya, S. K., Flesch, G. J., Mischna, M. A.,
975 Meslin, P.-Y., Farley, K. A., Conrad, P. G., Christensen, L. E., Pavlov,
976 A. A., et al., Jan. 2015. Mars methane detection and variability at Gale
977 crater. Science 347, 415–417.

978 Webster, C. R., Mahaffy, P. R., Atreya, S. K., Moores, J. E., Flesch, G. J.,
979 Malespin, C., McKay, C. P., Martinez, G., Smith, C. L., Martin-Torres,
980 J., Gomez-Elvira, J., Zorzano, M.-P., Wong, M. H., Trainer, M. G., Steele,
981 A., Archer, D., Sutter, B., Coll, P. J., Freissinet, C., Meslin, P.-Y., Gough,
982 R. V., House, C. H., Pavlov, A., Eigenbrode, J. L., Glavin, D. P., Pear-
983 son, J. C., Keymeulen, D., Christensen, L. E., Schwenzer, S. P., Navarro-
984 Gonzalez, R., Pla-García, J., Rafkin, S. C. R., Vicente-Retortillo, Á., Ka-
985 hanpää, H., Viudez-Moreiras, D., Smith, M. D., Harri, A.-M., Genzer,
986 M., Hassler, D. M., Lemmon, M., Crisp, J., Sander, S. P., Zurek, R. W.,

Vasavada, A. R., Jun. 2018. Background levels of methane in Mars' atmosphere show strong seasonal variations. Science 360, 1093–1096.

Wilzewski, J. S., Gordon, I. E., Kochanov, R. V., Hill, C., Rothman, L. S., Jan. 2016. H_2, He, and CO_2 line-broadening coefficients, pressure shifts and temperature-dependence exponents for the HITRAN database. Part 1: SO_2, NH_3, HF, HCl, OCS and C_2H_2. J. Quant. Spectrosc. Radiat. Transfer 168, 193–206.

Wunch, D., Toon, G. C., Blavier, J. L., Washenfelder, R. A., Notholt, J., Connor, B. J., Griffith, D. W. T., Sherlock, V., Wennberg, P. O., May 2011. The Total Carbon Column Observing Network. Phil. Trans. R. Soc. A 369, 2087–2112.

Yokota, T., Yoshida, Y., Eguchi, N., Ota, Y., Tanaka, T., Watanabe, H., Maksyutov, S., 2009. Global concentrations of co_2 and ch_4 retrieved from gosat: First preliminary results. Sci. Online Lett. Atmos. 5, 160–163.

Zak, E., Tennyson, J., Polyansky, O. L., Lodi, L., Zobov, N. F., Tashkun, S. A., Perevalov, V. I., Jul. 2016. A room temperature CO_2 line list with ab initio computed intensities. J. Quant. Spectrosc. Radiat. Transfer 177, 31–42.

Zurek, R. W., Chicarro, A., Allen, M. A., Bertaux, J.-L., Clancy, R. T., Daerden, F., Formisano, V., Garvin, J. B., Neukum, G., Smith, M. D., Feb. 2011. Assessment of a 2016 mission concept: The search for trace gases in the atmosphere of Mars. Planet. Space Sci. 59, 284–291.

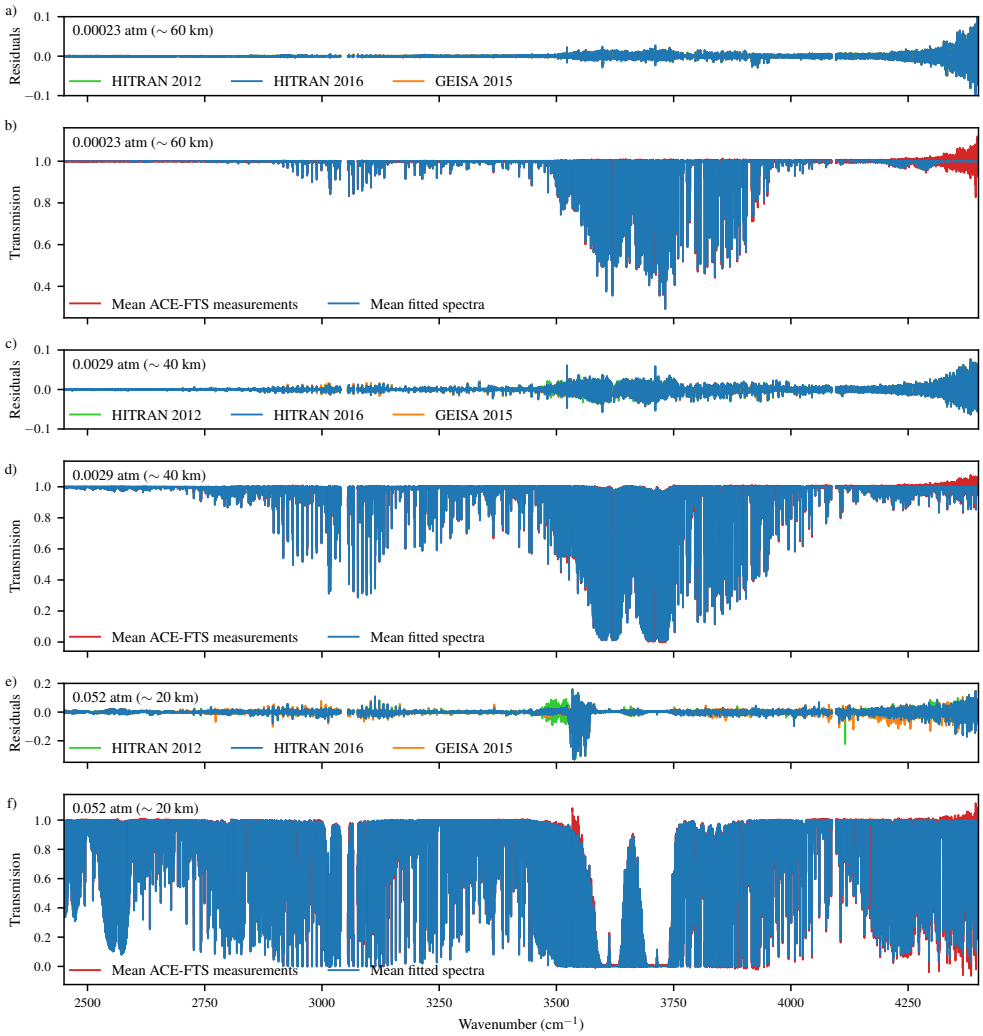

Figure 2: Mean ACE-FTS spectra, mean best-fit computed spectra, and mean residuals for each fitting window. Mean residuals are shown using HITRAN 2012 (green), HITRAN 2016 (blue) and GEISA 2015 (orange). Mean fitted spectra are shown only for when using HITRAN 2016. a) mean residuals from 0.00023 atm ($\sim$ 60 km), b) mean spectra and mean fits from 0.00023 atm, c) mean residuals from 0.0029 atm ($\sim$ 40 km), d) mean spectra and mean fits from 0.0029 atm, e) mean residuals from 0.052 atm ($\sim$ 20 km), f) mean spectra and mean fits from 0.052 atm.

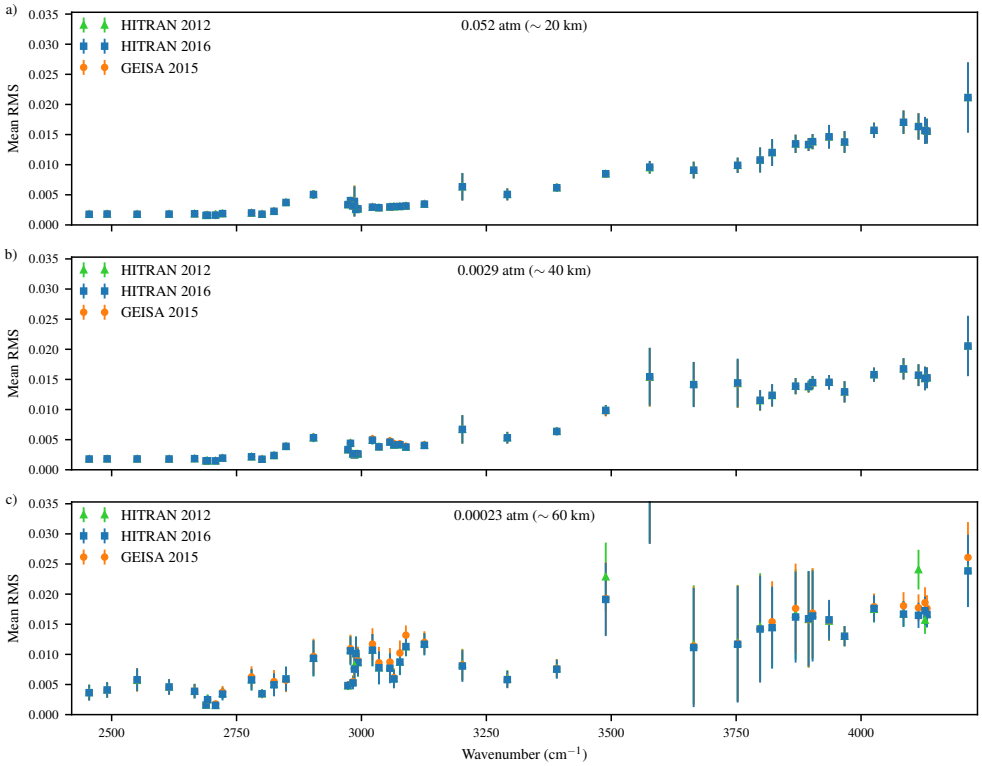

Figure 3: Mean RMS values computes for each fitting window when using each HITRAN 2012, HITRAN 2016, and GEISA 2015 at three pressure levels: a) 0.00023 atm ($\sim$ 60 km), b) 0.0029 atm ($\sim$ 40 km), c) 0.052 atm ($\sim$ 20 km).

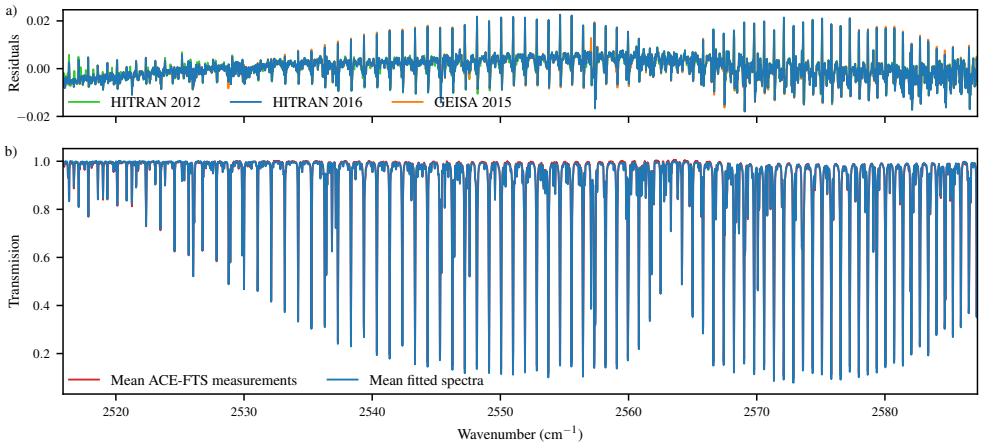

Figure 4: a) Mean residuals for the 2551.55 cm^{-1} window at 0.052 atm ($\sim$ 20 km) with HITRAN 2012, HITRAN 2016, and GEISA 2015. b) Mean measured ACE-FTS spectrum and mean computed spectrum (for HITRAN 2016). The primary features in this window are N_2O lines and the residuals correspond to the N_2O lines.

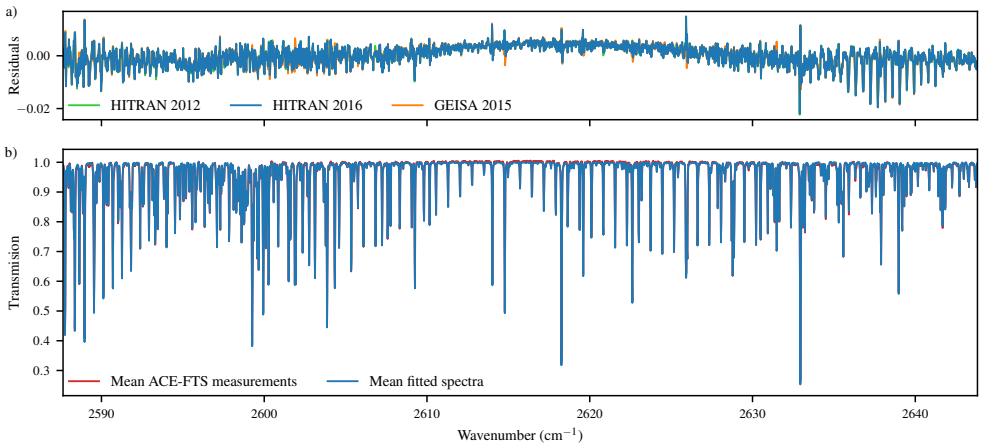

Figure 5: a) Mean residuals for the 2615.74 cm^{-1} window at 0.052 atm ($\sim$ 20 km) with HITRAN 2012, HITRAN 2016, and GEISA 2015. b) Mean measured ACE-FTS spectrum and mean computed spectrum (for HITRAN 2016). The main features are from N_2O towards the left edge, a CO_2 band across the entire window, and several strong CH_4 lines. The residuals are due to HNO_3.

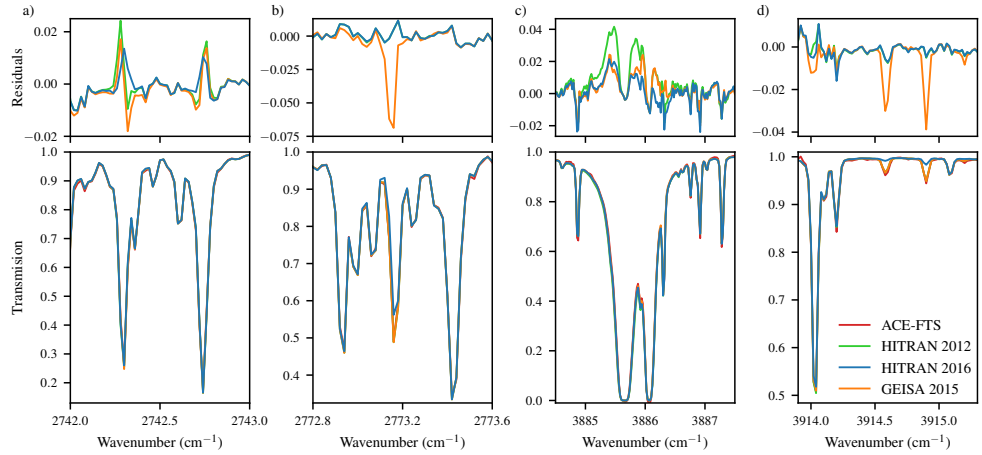

Figure 6: Zoom of the residuals and mean spectra (as in Figures 4 and 5) where errors are present, for the windows: a) 2722.25 cm^{-1}, b) 2780.74 cm^{-1}, c) 3869.14 cm^{-1}, d) 3936.15 cm^{-1}.

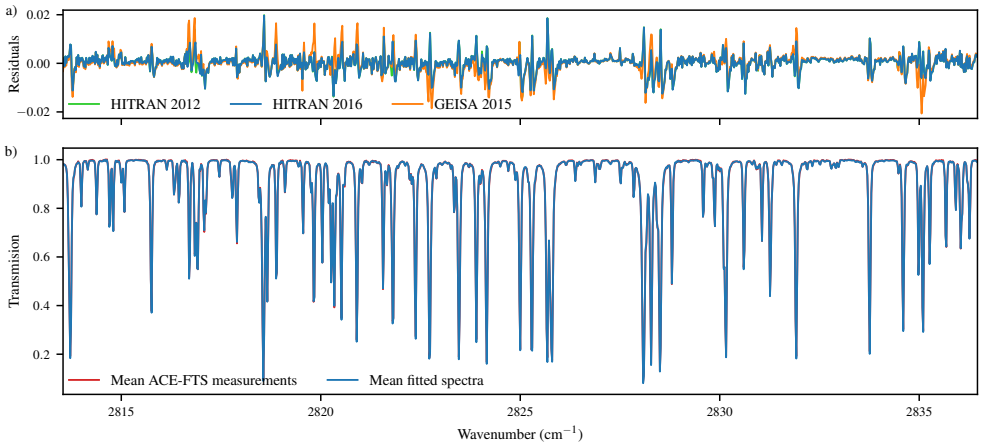

Figure 7: a) Mean residuals for the 2825.0 cm^{-1} window at 0.052 atm ($\sim$ 20 km) with HITRAN 2012, HITRAN 2016, and GEISA 2015. b) Mean measured ACE-FTS spectrum and mean computed spectrum (for HITRAN 2016). Features are primarily CH_4 lines.

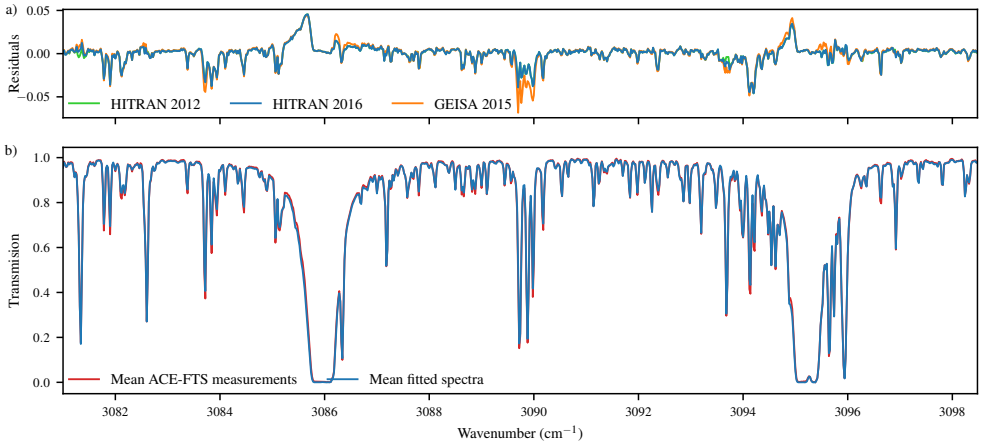

Figure 8: a) Mean residuals for the 3089.75 cm^{-1} window at 0.052 atm ($\sim$ 20 km) with HITRAN 2012, HITRAN 2016, and GEISA 2015. b) Mean measured ACE-FTS spectrum and mean computed spectrum (for HITRAN 2016). Absorption are due to, in order of prominence, CH_4, H_2O, and O_3. Large residuals near 3090 cm^{-1} are from CH_4 lines.

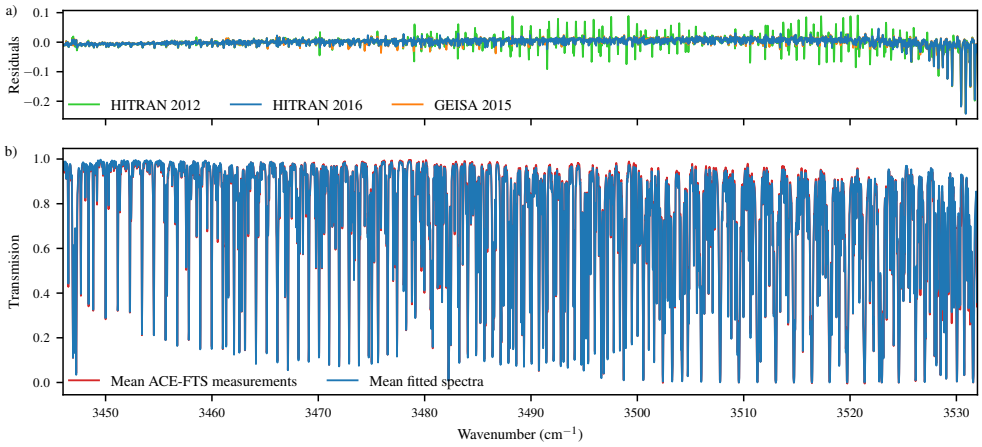

Figure 9: a) Mean residuals for the 3489.0 cm^{-1} window at 0.052 atm ($\sim$ 20 km) with HITRAN 2012, HITRAN 2016, and GEISA 2015. b) Mean measured ACE-FTS spectrum and mean computed spectrum (for HITRAN 2016). The primary features are an N_2O band on the left side, CO_2 bands on the right, and several H_2O lines. The strong residuals are due to CO_2 when using the HITRAN 2012 line list.

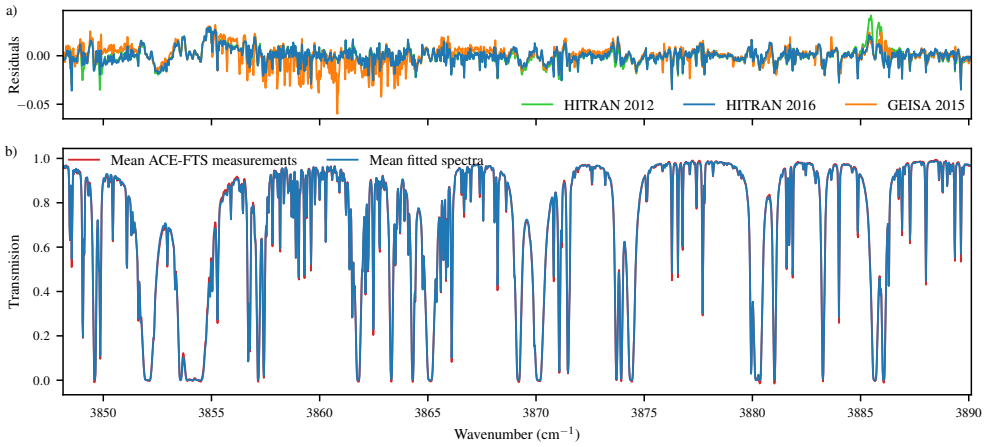

Figure 10: a) Mean residuals for the 3869.14 cm^{-1} window at 0.052 atm ($\sim$ 20 km) with HITRAN 2012, HITRAN 2016, and GEISA 2015. b) Mean measured ACE-FTS spectrum and mean computed spectrum (for HITRAN 2016). The primary features are H_2O lines. The strong residuals near 3860 cm^{-1} are due to O_3 when using GEISA 2015. Those near 3886 cm^{-1} are due to H_2O and are shown in Figure 6c.